NTNU
Norwegian University of
Science and Technology

Energy measurements at Ylja Hydropower Plant

Trine Brath

Master of Science in Mechanical Engineering
Submission date: June 2018
Supervisor: Bjørnar Svingen, EPT

Norwegian University of Science and Technology
Department of Energy and Process Engineering

NTNU
Norwegian University
of Science and Technology

Department of Energy
and Process Engineering

EPT-M-2018-12

MASTER THESIS

for

Student Trine Brath

Spring 2018

Energy measurement in the field

Energimåling i felt

Background and objective

The energy in the channel after a Pelton turbine is not homogenous in a cross section. Local patches of high and low energy exists, but better mix exists the longer away from the turbine the measurements are done. The energy consists of velocity and temperature. This non-homogenous mixture can result in errors when doing thermodynamic measurements.

In this Master thesis, field measurements shall be done. Ylja (Edsiva) has given a "go" for measurements in the outlet, and reports from earlier efficiency measurements exist. Temperature-measurements in the outlet shall be done with a frame that can be moved up/down and back/forth. Propeller current measurements shall be taken simultaneously. These measurements can preferably be combined with thermodynamic efficiency measurements, ie. install a temperature sensor on the inlet as well. The candidate will be assisted with this part. Data from the measurements in the outlet shall be analyzed with respect to flow, temperature and error analysis for thermodynamic efficiency measurements.

It must be noted that these measurements are to be taken in the field, on a "live" power plant. Thus, placement of the frame in the outlet must be done as best as possible.

If the student will go to Nepal for a excursion, earlier and further work will be presented as a publication and presented at the conference; 8th *International symposium on Current Research in Hydraulic Turbines (CRHT-VIII)* at Kathmandu University in March 2018.

The following tasks are to be considered:

1 Gather information from Ylja powerplant, especially the outlet, and get in contact with the contact person.
2 The frame will be made by Rainpower, but assistance for fastening of the current meters is needed.
3 Plan the measurements
4 Execute the measurements
5 Eventually travel to Nepal and make a publication
6 Analyze the results with respect to flow, temperature and error analysis
7 Write a report

NB! The sequence above is not necessarily chronological. The points 1, 2 and 3 must be done ASAP, so that the measurements can be done in the spring.

-- " --

Within 14 days of receiving the written text on the master thesis, the candidate shall submit a research plan for his project to the department.

When the thesis is evaluated, emphasis is put on processing of the results, and that they are presented in tabular and/or graphic form in a clear manner, and that they are analyzed carefully.

The thesis should be formulated as a research report with summary both in English and Norwegian, conclusion, literature references, table of contents etc. During the preparation of the text, the candidate should make an effort to produce a well-structured and easily readable report. In order to ease the evaluation of the thesis, it is important that the cross-references are correct. In the making of the report, strong emphasis should be placed on both a thorough discussion of the results and an orderly presentation.

The candidate is requested to initiate and keep close contact with his/her academic supervisor(s) throughout the working period. The candidate must follow the rules and regulations of NTNU as well as passive directions given by the Department of Energy and Process Engineering.

Risk assessment of the candidate's work shall be carried out according to the department's procedures. The risk assessment must be documented and included as part of the final report. Events related to the candidate's work adversely affecting the health, safety or security, must be documented and included as part of the final report. If the documentation on risk assessment represents a large number of pages, the full version is to be submitted electronically to the supervisor and an excerpt is included in the report.

Pursuant to "Regulations concerning the supplementary provisions to the technology study program/Master of Science" at NTNU §20, the Department reserves the permission to utilize all the results and data for teaching and research purposes as well as in future publications.

The final report is to be submitted digitally in DAIM. An executive summary of the thesis including title, student's name, supervisor's name, year, department name, and NTNU's logo and name, shall be submitted to the department as a separate pdf file. Based on an agreement with the supervisor, the final report and other material and documents may be given to the supervisor in digital format.

☐ Work to be done in lab (Water power lab, Fluids engineering lab, Thermal engineering lab)
☒ Field work

Department of Energy and Process Engineering, 15. January 2018

Bjørnar Svingen
Academic Supervisor

Research Advisor: Henning Lysaker

Abstract

The purpose of this master thesis was to take fieldmeasurements and find the energy distribution in the cross section at different distances from a Pelton turbine. According to IEC60041: 1991, thermodynamic efficiency measurements on Pelton turbines shall be done from 4 to 10 runner diameters away from the turbine center. This is due to inhomogeneous energy distribution.

For several reasons the assignment was changed. The new purpose was to measure the energy in a cross section with different numbers of injectors running, and see if and how the distribution changed. An uncertainty analysis was also made. The measurements were done at Ylja hydropower plant, and the energy was found by measuring the temperature. To measure the temperature, three SeaBird SBE38 sensors were used. The temperature was measured in 7 points in the cross section.

The measurements showed that the energy distribution in the outlet of a Pelton turbine was not homogeneous. Some areas in the cross section had a higher temperature than others. Could see some patterns in the energy distribution, but it changed according to the number of injectors that were running. Measurements and observations showed that in the upper layer of the outlet channel flow air and water were mixed together. Measurements in this area will give false values of the water temperature because the air heats up the water. Weighing all temperature measurements equally when finding the thermodynamic efficiency gives greater uncertainty and can give an incorrect result. To find out how much to weigh the different measurements, one must find the velocity distribution.

Sammendrag

Formålet med masteroppgaven var å gjøre målinger i felt og finne energifordelingen i tverrsnittet ved forskjellige distanser fra en Pelton turbin. I henhold til IEC60041:1991 skal termodynamiske virkningsgradmålinger på Pelton turbiner gjøres 4-10 løpehjuldiametere fra turbines sentrum grunnet inhomogen energifordeling.

Av flere årsaker ble oppgaven forandret. Det nye formålet var å måle energien i ett tverrsnitt når forskjellig antall dyser blir kjørt, og se om fordelingen endret seg. Ble og gjort en usikkerhetsanalyse. Målingene ble gjort på Ylja kraftverk, og energien ble målt ved temperatur. For å måle temperaturen ble tre SeaBird SBE38 sensorer brukt. Temperaturen ble målt 7 steder i tverrsnittet.

Målingene viste at energifordelingen i utløpet på en Pelton turbin ikke var homogen. Noen områder i tverrsnittet har høyere temperatur enn andre. Kunne se et mønster på hvordan temperaturen oftest utarter seg i tverrsnittet, men det forandret seg etter antall dyser som ble kjørt. Målinger og observasjoner viste og at i det øverste området av utløpsstrømmen ble luft og vann mikset sammen. Målinger i dette området vil gi et uriktig bilde av vannets temperatur fordi luften varmer opp vannet. Å vekte alle temperaturmålingene likt når man skal finne den termodynamiske virkningsgraden gir større usikkerhet og kan gi et uriktig resultat. For å finne ut hvor mye man skal vekte de ulike målingene må man finne hastighetsfordelingen.

Preface

The following work is a result of a master thesis carried out at the Water Power Laboratory at the Norwegian University of Science and Technology in the spring of 2018. Some changes were made to the initial assignment. Instead of measuring the energy in different cross sections, the energy would be measured in one cross section when different numbers of injectors are running.

I would like to thank my supervisor Associated Professor Bjørnar Svingen and my co-supervisor Henning Lysaker from Rainpower for all the guidance and advice I have gotten during the entire process. A big thank you to Eidsiva Energi AS and Frank Mo who let me take measurements at Ylja Hydropower Plant. Special thanks to Nils Olav Dalåker, Leif Søndrol and Knut H. Berg who helped me rig up and take down my equipment at Ylja Hydropower Plant. I would also like to thank my dad for his input in designing the measurement frame, and my mom for proof reading the master thesis. I would also like to thank my fellow students at the laboratory for creating a positive work environment.

Trondheim, 2018-06-08

Trine Brath

Contents

List of Figures

List of Tables

Nomenclature

Symbols	Term	Unit
η	Hydraulic efficiency	[-]
P	Power	[MW]
E	Specific energy	[J]
Q	Discharge (volume flow rate)	[m^3/s]
A	Area	[m^2]
D	Inlet pipe diameter	[m]
W	Outlet channel width	[m]
L	Height of water in outlet channel	[m]
g	Gravitational acceleration	[m/s^2]
ρ	Density	[kg/m^3]
cp	Specific heat capacity	[J/(kgK)]
$\bar{a}$	Isothermal factor	[m^2/kg]
Δ	Difference	[-]
p	Pressure	[Pa]
c	Velocity	[m/s]
z	Elevation	[m]
T	Temperature	[$^\circ C$]
h	Height from sensor to water surface	[m]
ν	Kinematic viscosity	[m^2/s]
τ_w	Wall shear stress	[$kg/(ms^2)$]
y^+	Dimensionless wall coordinate	[-]
u^+	Dimensionless velocity	[-]

Symbols	Term	Unit
u_τ	Friction velocity	[m/s]
κ	von Kármán constant	[-]
C^+	Constant	[-]
σ	Standard deviation	[-]
s_Y	Estimated standard deviation	[-]
Y_i	Value of one measurement	[-]
$\bar{Y}$	Mean value of measurements	[-]
N	Number of measurements	[-]
t_{95}	Student t factor for 95% confidence interval	[-]
f	Relative uncertainty	[%]
e	Absolute uncertainty	[-]

Subscripts and abbreviations	
gen	Generator
$turb$	Turbine
h	Hydraulic
m	Mechanical
p	Pressure
kin	Kinetic
pot	Potential
T	Thermal
atm	Atmospheric
s	Systematic
r	Random
1	Turbine inlet center
$1-1$	Measuring point turbine inlet
2	Turbine outlet center
$2-1$	Measuring point turbine outlet

Chapter 1

Introduction

1.1 Background

For people working in the hydropower business it is important to know the efficiency of the hydropower plant. The efficiency is defined as the ratio between the power produced and the power put into the system. The higher the efficiency, the less energy is lost, and more money is earned.

For efficiency measurements in the field the standard used is "IEC 41:1991: Field acceptance tests to determine the hydraulic performance of hydraulic turbines, storage pumps and pump turbine". When doing a thermodynamic efficiency measurement on a Pelton turbine IEC 41 requires that that the measurements at the outlet are made somewhere between 4 and 10 runner diameters away from the turbine. It can sometimes be difficult to get to these areas of the channel, and measurements are therefore done at a distance of , for example, 2 or 3 runner diameters from the turbine. This is not correct according to IEC 41 and the efficiency measurements could be invalid.

The reason why IEC 41 states that the measurement has to be done at 4-10 runner diameters is because the energy in the channel after a Pelton turbine is not homogeneous. There are local areas in the cross section with high and low energy. In the upper layer of the outlet flow water and air is mixed, creating a "foam" layer, which does not

have the same energy as the rest of the flow because the air has a higher temperature than the water. The energy becomes more mixed further away from the turbine. The energy in this case are velocity and temperature. Measuring at a cross section where the energy is not homogeneous can lead to inaccuracies in the thermodynamic efficiency measurements. It is therefore important to measure at cross sections where the energy is mixed well enough.

1.2 Objective

The objective of this master thesis was to measure the energy at different cross sections in the outlet of a Pelton turbine, and analyze the data to see how much the distance from the turbine center has to say on the thermodynamic efficiency measurements. Field measurements were to be done in the outlet of a Pelton turbine. To find the energy in the cross section the outlet velocity, and the outlet and inlet temperature were to be measured. Ylja power plant has a Pelton turbine and Eidsiva Energi AS gave permission to use the power plant to do measurements.

Few have done measurements to see how the distance from the turbine affect the thermodynamic efficiency. During the literature study for this master thesis a report presented at The 7th International Conference on Hydraulic Efficiency Measurements in Milan, Italy in 2008 by Harald Hulaas, Erik Nilsen and Leif Vinnogg from Norconsult, Norway and Eirik Bøkko from E-CO Vannkraft, Norway was found. In their report they concluded that the distance from the turbine centre to the measuring section was important, and that the minimum distance set in IEC 41 should be the minimum. Part of the objective of this thesis was to investigate their conclusion.

1.3 Changes in objective

The measurements in this master thesis are not in direct accordance with the orginial objective. After an excursion to Ylja hydropower plant and after rigging up the equip-

ment the objective of this master thesis changed. Instead of measuring the energy at different cross sections, the energy was measured at one cross section, and while running different numbers of injectors and at different power settings. The energy was only measured in form of the temperature. The objective changed to finding the energy and see if and how it changes in the cross section, and also see if and how the energy distribution changes when the number of injectors running and the power increase. An error analysis would also be done. The reasons for these changes in objective was because it was not possible to measure at different distances from the turbine, and the sensors that would measure the velocity stopped working.

1.4 Short description of Ylja power plant

Ylja hydropower plant is owned by Oppland Energi AS, which is partially owned by Eidsiva AS. Permission to take measurements at Ylja power plant was given by Eidsiva Energi AS. It is located in Vang municipality and gets water from two reservoirs and six additional streams.

Turbine type	Pelton
Turbine manufacturer	Kværner
Shaft	Vertical
Rated turbine power	65 MW
Nominal head	687 m
Flow rate (fulload)	12 m^3/s
Commissioned	1973

Table 1.1: Information about Ylja [15]

Earlier efficiency measurements:

- 1982, November, Kværner, P. Schancke, Eirik Bøkko

- 2008, April, E-CO Vannkraft AS, Atle Lundekvam, Eirik Bøkko

1.4.1 People involved

The people who were involved in the measurements were:

- Trine Brath, author of this master thesis
- Bjørnar Svingen, supervisor
- Vegard Ulvan, co-student
- Nils Olav Dalåker, technician from Eidsiva Energi AS
- Leif Søndrol, technician from Eidsiva Energi AS
- Knut H. Berg, technician from Eidsiva Energi AS

Chapter 2

Basic theory

2.1 Thermodynamic efficiency measurements

The thermodynamic method is a method for measuring the efficiency of a hydraulic turbine. It uses the principle of conservation of energy, and uses parameters such as pressure (p), temperature (T), velocity (c) and defined elevations (z) and the thermodynamic properties of the water. The efficiency is generally defined as in equation (2.1).

$$\eta = \frac{P_{produced}}{P_{available}} = \frac{E_m}{E_h} \tag{2.1}$$

Where E_m is the mechanical energy, and E_h is the total hydraulic energy that theoretically can be collected from the water.

$$\begin{aligned} E_m &= E_{m,pressure} + E_{m,kinetic} + E_{m,potential} + E_{m,thermal} + \delta E_m \\ &= \bar{a}(p_{1-1} - p_{2-1}) + \frac{1}{2}(c_{1-1}^2 - c_{2-1}^2) + g(z_{1-1} - z_{2-1}) + \bar{cp}(T_{1-1} - T_{2-1}) + \delta E_m \end{aligned} \tag{2.2}$$

$$\begin{aligned} E_h &= E_{h,pressure} + E_{h,kinetic} + E_{h,potential} \\ &= \frac{1}{\bar{\rho}}(p_1 - p_2) + \frac{1}{2}(c_1^2 - c_2^2) + g(z_1 - z_2) \end{aligned} \tag{2.3}$$

The primary parameter for determining the mechanical energy is the water temperature. The losses in the turbine will cause the temperature in the water to increase. This difference can be used to measure the energy, and thereby the turbines efficiency. If the temperature variation is small, the velocity distribution does not matter [6].

The accuracy of the thermodynamic method increases with the amount of mechanical energy that is measured. The method is therefore preferably used for high-head turbines ($head \geq 100m$), such as Pelton turbines, as stated in IEC 41 [10].

The IEC 41 gives a lot of specifications on how to take the measurements. One condition is that for a Pelton turbine, which has a channel with a free surface, the distance between the turbine and the outlet measuring section should be 4 to 10 runner diameters [10]. This is because for Pelton turbines there has been an issue on how well the water is mixing in the tail race [6]. A distance of 4 to 10 runner diameters will ensure an adequate mixing of water without having significant heat exchange with surroundings.

In a report made by Norconsult and E-CO for IGHEM in Milan, Italy 2008 [6] it is stated that Pelton turbines with a horizontal shaft have a more even energy distribution than the ones with a vertical shaft. The reason for this is thought to be due to the more symmetrical discharge pattern into the pit from a horizontal shaft turbine. In the report it also says that it clearly appears that sufficient distance from measuring section to turbine centre is important to reduce the uncertainty.

2.1.1 Temperature measurements

A lot of energy has to be added to the water to increase the temperature because water has a high heat capacity. The increase in temperature from inlet to outlet of the turbine is therefore very small. This poses great demands on the sensitivity of the temperature sensors. They must be able to measure changes down to one-thousandths of a degree Celsius. When exploring the temperature variation in the cross section at least 6 points should be used. The calculated efficiency should not deviate more than 1.5% between any two points [6]. Hulaas and Dahlhaug did a comparison of energy measurements from Bratsberg Hydropower plant and Kaldestad hydropower plant to examine how many measurement points there had to be in the outlet to get satisfactory

uncertainties. The study showed that to get a 95% confidence interval under 0,6% of the mechanical energy at least 5 measurement points are needed [5].

There are different ways of measuring the temperature in the outlet. One way is to use a horizontal "sampling beam" which is held in different depths. The "sampling beam" takes water from 4 or more points distributed over the channel, and leads the water to a central mixing chamber where a temperature sensor measures the average temperature over the width. Another method is to place three or more vertical perforated pipes from the channel bottom up to the deck over the canal. The temperature sensors are then placed inside the pipes and can be placed at different elevations. According to a paper written by Hulaas, Nilsen, Vinnogg and Bøkko using horizontal sampling branch pipes gives a good average of the energy distribution, but the extremes are better mapped with perforated standing pipes [6].

For a Pelton turbine the outlet is a free surface channel. When the water exits the turbine it will be mixed with the air. The upper layer of the channel flow will therefore have entrained air ("foam"). There will be a heat exchange between the air and the water, and temperature measurements in this layer are not representative for the water temperature. How large the foam layer is is difficult to say. It varies the velocity.

2.1.2 Velocity measurements

To measure the flow velocity a current meter can be used. A current meter is a device that measures the flow by mechanical, tilt, acoustical or electromagnetic induction. Mechanical current meters are based on counting the rotations of a propeller, and therefore called propeller current meters or rotor current meters. More about propeller current meter can be read about in the project thesis "Energy measurements in a free surface channel" [3].

Magnetic flow meters are current meters that use Faraday's law of electromagnetic induction to measure the velocity of the water. The principle of Faraday's law of electromagnetic induction is that a conductor moving through a magnetic field generates voltage, which is proportional to the speed of the movement. An alternating current passes a coil in the sensor, and a magnetic field is put up in and around the sensor.

Water is a conductor, and when the water passes the sensor voltage is produced. This voltage is a measurement of the waters velocity [20].

The velocity of the flow in a free surface channel cross section varies. It varies with the depth from the free surface and the distance from the sides of the channel. This is due to shear stress at the bottom and at the sides of the channel and due to the presence of free surface [7]. The velocity components in the vertical and transverse direction are usually small and can be neglected. Therefore, only the velocity component in the flow direction is considered. The shear stress at the channel walls gives the no-slip condition. The no-slip condition says that the velocity at the wall must be zero, or the same as the walls velocity. The velocity of the fluid must increase therefrom for movement to take place. When the flow is turbulent finding the velocity distribution is complicated due to the powers of the an-isotropic turbulence that involve the Prandtl's second type of secondary flow occurring in the cross section. With these currents the maximum velocity appears below the free surface, this is called a dip phenomenon[2].

The area closest to the wall, called inner layer, can be divided into three regions. The viscous sub-layer ($y^+ < 5$), the buffer layer ($5 < y^+ < 30$) and the log-law region ($y^+ > 30$). In 1930 Theodore von Kármán published "The Law of the Wall". The law of the wall says that the average velocity of a turbulent flow at a certain point is proportional to the logarithm of the distance from that point to the wall, or the boundary of the fluid region [19].

$$u^+ = \frac{1}{\kappa} \ln y^+ + C^+ \tag{2.4}$$

with $y^+ = \frac{y u_\tau}{\nu}$, and $u_\tau = \sqrt{\frac{\tau_w}{\rho}}$, and $u^+ = \frac{u}{u_\tau}$

Equation (2.4) is only valid in the log-law region, and when the surface is smooth. In the viscous sub-layer the flow must be laminar, regardless of what the flow is elsewhere. This is because of the no-slip condition. The thickness of this layer depends on how deeply the turbulent perturbations penetrate the layer [4]. Here it is approximated that:

$$u^+ = y^+ \tag{2.5}$$

In the buffer layer the velocity profile is neither logarithmic or linear, so neither equation(2.4) and (2.5) can be used. Instead the velocity profile is a merge between the two.

Outside the inner layer, in the outer layer, the velocity distribution can not be described with the law of the wall. Here the velocity distribution can be found by Navier-Stokes equations or with experiments.

The outlet channel of a Pelton turbine is cut out of the mountain, and the surface roughness of the walls are therefore very large. Equation 2.4 will therefore not be valid. With increased surface roughness the turbulence near the wall is increased and gets more complex. This in turn has significant effect on the momentum, heat and mass transfer rates at the surface, since they are controlled by the turbulent flow structure in the near-wall region [1]

2.2 Uncertainty analysis

When doing measurements there will be a difference in the measurements and the true value of the measured quantity. This difference is called an error and can be divided into three types.

- Spurious errors
- Random errors
- Systematic error

Spurious error

Spurious errors are errors such as human errors or instrument malfunction. These errors should not be incorporated into any statistical analysis and the measurement must be discarded.

Random error

Random errors are caused by numerous, small, independent influences which prevent a measurement system from delivering the same quantity as the real quantity over several measurements. These errors behave in a statistical pattern, and usually approaches a normal (Gaussian) distribution as the number of measurements are increased. The mean value is a better estimate of the real value, than an individual measurement. To calculate the uncertainty in the mean value it is necessary to calculate the standard deviation and decide on a confidence level. IEC 41 uses a 95% confidence level. Because the exact value of σ is not known, the estimation s_Y is used instead.

$$s_Y = \sqrt{\frac{\sum_{i=1}^{N}(Y_i - \bar{Y})^2}{N-1}} \tag{2.6}$$

where Y_i is the value of one observation, $\bar{Y}$ is the mean of the observations, and N is the number of measurements. Equation 2.7 shows how to calculate the random uncertainty:

$$e_r = \frac{t_{95} s_Y}{\sqrt{N}} \tag{2.7}$$

where t_{95} is the student t factor for a 95% confidence interval. IEC 41 provides tables with values of the student t factor. More about probability distribution, standard deviation and confidence interval can be read about in the project thesis "Energy measurements in a free surface channel" [3].

Systematic error

Systematic errors are those which cannot be reduced by increasing the number of measurements if the equipment and conditions of the measurements remain unchanged. These errors comes from poor calibration, environmental interference, something wrong with the equipment or incorrect use of the equipment.

The total uncertainty of a measurement is obtained by combining the random error and the systematic error.

$$f_{total} = \pm\sqrt{(f_{random}^2 + f_{systematic}^2)} \tag{2.8}$$

A measurement system is often made up of a chain of components, each of which is subject to individual inaccuracy [8]. R is to be computed, where R is a function of n independent variables, u_1, u_2, ... u_n, as given in equation 2.9,

$$R = f(u_1, u_2, ..., u_n) \tag{2.9}$$

The u's are measured values, and each of the values are accompanied by an error Δu. Together these errors will cause an error ΔR in R.

$$R \pm \Delta R = f(u_1 \pm \Delta u_1, u_2 \pm \Delta u_2, ..., u_n \pm \Delta u_n) \tag{2.10}$$

An equation for the maximum absolute error in R can be found by expanding f as a Taylor expansion, as shown in equation 2.11, and neglecting the higher order terms. The higher order terms can be neglected because in practice the $\Delta u's$ are small quantities [8].

$$f(u_1 \pm \Delta u_1, u_2 \pm \Delta u_2, ..., u_n \pm \Delta u_n) = f(u_1, u_2, ..., u_n) + (\left|\frac{\partial f}{\partial u_1}\right|\Delta u_1 + \left|\frac{\partial f}{\partial u_2}\right|\Delta u_2 + ... + \left|\frac{\partial f}{u_n}\right|\Delta u_n) \tag{2.11}$$

$$\Rightarrow |\Delta R| = \left|\frac{\partial f}{\partial u_1}\right|\Delta u_1 + \left|\frac{\partial f}{\partial u_2}\right|\Delta u_2 + ... + \left|\frac{\partial f}{u_n}\right|\Delta u_n \tag{2.12}$$

The form of equation 2.12 is very useful since it shows which variables exerts the strongest influence on the accuracy of the overall result. If $\partial f/\partial u_2$ is large compared to the other partial derivatives then a small Δu_2 will have a large effect on the total ΔR.

By treating the individual errors as statistical bounds for the individual variables, the probable total change in R caused by the individual errors can be expressed by the Root-sum-square method as shown in equation 2.13 [17].

$$\Delta R = \pm\sqrt{(\frac{\partial f}{\partial u_1}\Delta u_1)^2 + (\frac{\partial f}{\partial u_2}\Delta u_2)^2 + ... + (\frac{\partial f}{u_n}\Delta u_n)^2} \tag{2.13}$$

2.2.1 Thermodynamic uncertainty

The total uncertainty in the thermodynamic efficiency measurements can be found by the general equations in the section above. It is known that η is dependent on the mechanical energy and the hydraulic energy.

$$\eta = f(E_m, E_h) \tag{2.14}$$

Since E_m and E_h are found by measured values they will have an error, which gives an error in η. The total uncertainty of the measurement can be found by :

$$f_\eta = \sqrt{e_m^2 + e_h^2} \tag{2.15}$$

Where e_m and e_h are the absolute uncertainty of the mechanical and hydraulic energy, and consists of the systematic uncertainty and random uncertainty. More about the uncertainty analysis can be found in appendix D.

Chapter 3

Method

3.1 Excursion to Ylja

31st of January Bjørnar Svingen and Trine Brath travelled to Ylja hydropower plant to inspect the hydropower plant. After conversations with personnel from Eidsiva and studying the drawings, it was clear that emptying of the outlet tunnel would require too much resources and time. The outlet tunnel goes straight out into Strøndafjorden, and when the turbine is shut down there will always be a lot of water in the tunnel. It would therefore not be possible to move the measuring frame to different distances from the turbine. The measuring frame had to be positioned and fastened where the bridge over the outlet was. From this bridge the measuring frame could be hoisted down. There was no number on how far away from the turbine this location was, but from drawings, see figure 3.1, it could be seen that it was a little bit over two runner diameters from the turbine center. This is not within IEC 41 recommendations. Due to time restrictions it was not possible to find a new hydropower plant with a Pelton turbine. After discussions between Trine Brath, Bjørnar Svingen and Henning Lysaker it was decided that the energy would only be measured in one cross section, and the energy distribution would be found with different injectors running.

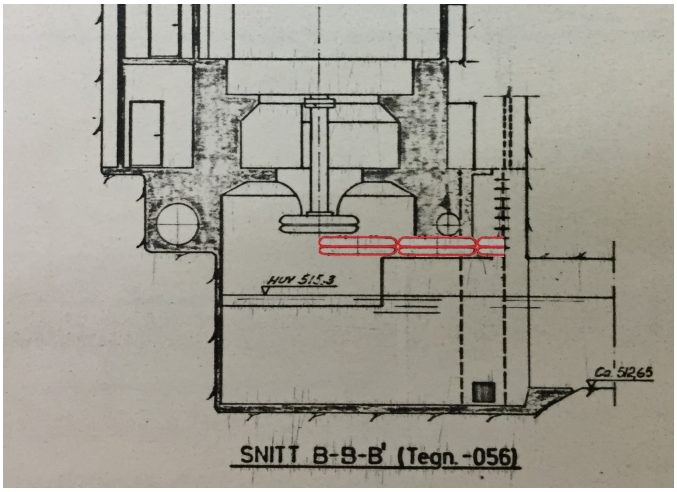

Figure 3.1: Distance from turbine to location for outlet measurements illustrated by red runners

Ylja hydropower plant did not have a meter to easily measure and log the power produced by the generator. The only way to know the power directly from the generator would therefore be to read off the display of the turbine governor. This is not precision measurement, but there was no other choice. In preparations of the field measurements the author of this thesis spent time studying the user manual and in the laboratory at Rainpower to learn how to use and control the turbine governor.

The efficiency measurements in 1983 had a problem with unstable inlet temperature. The turbine got water from an upper reservoir and six additional streams. The water from the streams had a different temperature than the water in the upper reservoir. To solve this they opened the stoplog, so the water from the streams wouldn't flow together with the water from the upper reservoir. In 1983 the measurements were done in the fall, and it was possible to get to the stoplog. In the winter because of the snow it was not possible to get to the stoplog. The inlet temperature could therefore end up being unstable. To be able to check if the inlet temperature was unstable it was decided to also measure the inlet temperature.

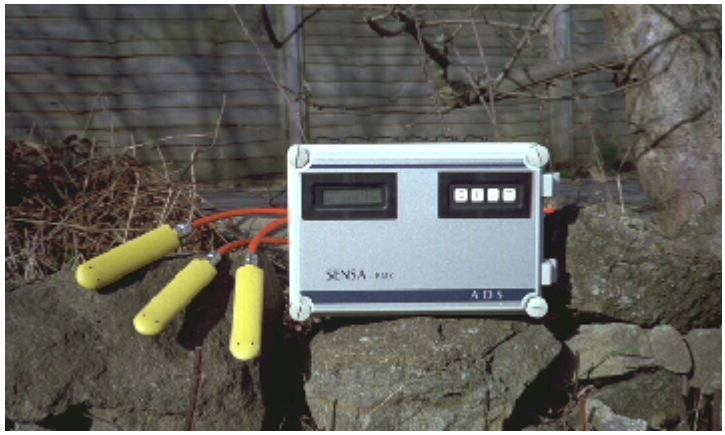

Figure 3.2: SENSA RV2 sensors and Aqua Data RMX (Picture from Aqua Data homepage)

3.2 Equipment

3.2.1 SENSA RMX and RV2

To measure the velocity SENSA RV2 sensors were used. The sensors, figure 3.2, are magnetic flow meters and are connected to a recording device, an Aqua Data RMX, which shows the measured velocity. To transfer the data to a computer a LabVIEW program was used. The program is attached in appendix B.

The SENSA RV2 sensors have an uncertainty of 0,5% and can be used to measure velocity between -8,0m/s and 8 m/s. The resolution is up to 1mm/s.

A propeller current meter is a more accurate device, but the decision to use magnetic flow meters instead of propeller current meters was made because it was not possible to get three or more propeller current meters. One or two propeller current meters would be too few, and the measurements would have taken too long. The Water Power Laboratory has 6 magnetic flow meters. They were all last calibrated 20th of March in 1995. To confirm that they were still working and giving the correct values a test was conducted in the free surface loop at the Water Power laboratory at NTNU. The sensors were placed in the same location in the channel to see if they showed the same velocity. A mini propeller current meter, borrowed from the Department of Civil and Environmental Engineering, was used as a reference. They were put 50 cm from the channel

Equipment	Calibration number	Mean velocity
SENSA RV2 sensor 1	46213277	0,1486 m/s
SENSA RV2 sensor 2	45814485	0,1441 m/s
SENSA RV2 sensor 3	46816785	0,1401 m/s
SENSA RV2 sensor 4	39817366	0,0756 m/s
SENSA RV2 sensor 5	45214265	0,1369 m/s
SENSA RV2 sensor 6	33319770	0,1924 m/s
Propeller current meter	-	0,1505 m/s

Table 3.1: Test of velocity measuring equipment

walls, and 45 cm from the bottom. The pump was running constantly at 530RPM. For each meter the velocity was measured for 1 minute 6 times. The averaged velocity in this point is showed in table 3.1.

From the test it was concluded that the SENSA RV2 sensor 4 and 6 could not be used. Chose to use SENSA RV2 sensors 1, 2 and 3 because they showed similar velocity, and were closest to the velocity found with the propeller current meter.

3.2.2 Sea-Bird SBE38

To measure the inlet and outlet temperature four SeaBird SBE38 sensors were used. The SBE38 sensors could not be calibrated at the Water Power Laboratory at NTNU, since the available calibration equipment had a higher uncertainty than the sensors themselves. The Water Power Laboratory has 5 SBE38 sensors. The manufacturer ensures $0.001°C$ or less uncertainty, but they were last calibrated in Washington 2003 [14]. To ascertain if the SBE38s were still showing correct values, and similar values between them, a small measurement test was done in the laboratory. On October the 25th a measurement test was conducted on the sensors by placing all the sensors in a insulated bucket with ice, figure (3.3). The previous calibration would be credible if the measurements closed in on $0°C$ and were similar to each other. The results showed that all the sensors closed in on $0°C$. Only ~ $0.003°C$ away from being zero. It was concluded that the calibration done in Washington is credible.

SeaBird SBE38 sensor with ID=01 (S/N 3844844-0315) was used at the inlet, and ID=02 (S/N 3832689-0199), ID=04 (S/N 3844844-0315) and ID=05 (S/N 3832689-0199)

Figure 3.3: Seabird 38 measurement test

Figure 3.4: Set-up with computers for temperature and velocity measurements

were used at the outlet.

3.2.3 Pressure

To measure the atmospheric pressure a UNIK 5000 pressure sensor (5 bar a) was used. To measure the inlet pressures two DigiQuartz pressure sensors (140 bar a) were used. Read more about the pressure measurements that were done at Ylja power plant in Veg-

ard Ulvan's master thesis "Pressure pulsations and efficiency measurements at Smeland Power Plant" [12], as he was the one responsible for the pressure measurements. The set up for the pressure measurements can be seen in figure 3.5.

Figure 3.5: Set-up pressure measurements

To decide the waters thermodynamic characteristic, water from the inlet pipe is drained with help from a specially designed probe, seen in figure 3.6.

3.2.4 Measurement frame

From earlier thermodynamic efficiency measurements, the hydropower plant had three perforated metal pipes, which had been used when measuring the outlet temperature, figure 3.7.

They measured 41mm in inner diameter. A Seabird SBE38 sensor is 40mm in outer diameter. The sensors would therefore fit into the pipes, but with little clearance. It was still decided that they would be used instead of making new ones. The three perforated pipes would stand almost vertically down into the channel. The pipes stood with a slight angle. How large the angle was was unknown until after the rig up. The angle turned out to be 1.37°. The temperature sensors could then be placed in various elevations in each of the pipes. Figure 3.8 shows a sketch of the measurement pipes.

Figure 3.6: Inlet probe

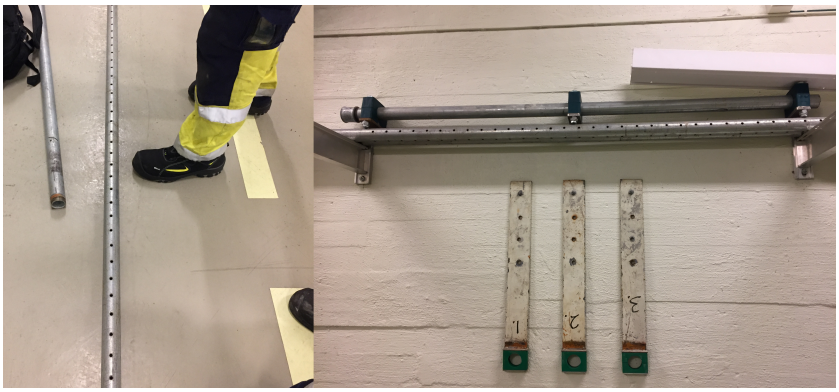

Figure 3.7: Perforated metal pipes

The hydropower plant did not have a measuring frame where the SENSA RV2 sensors could be fastened. It had to be made. The technicians at Rainpower built a frame after a design made by Trine Brath. A sketch of the frame can be seen in figure 3.9. More sketches are found in appendix A.

The frame was made out of 5 parts. The main frame was made from steel and was

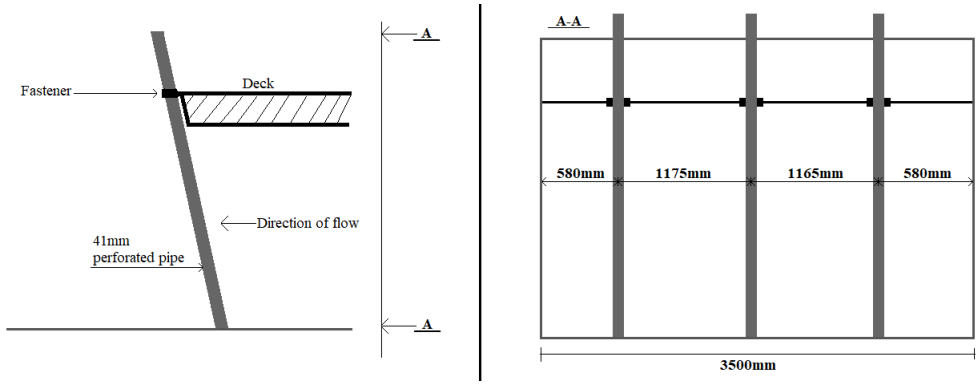

Figure 3.8: Sketch of temperature measurement pipes

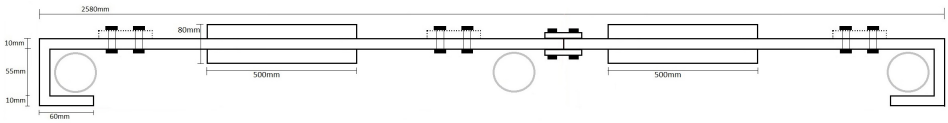

Figure 3.9: Sketch of velocity measuring frame, seen from above.

cut in two to make transportation easier. Three aluminum plates were made to hold the SENSA sensors. These plates would be screwed to the main frame. The end of the frame went around the perforated metal pipes as a way to hold the frame in place. Two slightly angled plates at the middle of the frame would ensure that the frame was pushed down by the water and kept still against the vertical pipes. A rope was fastened in both ends of the frame to be able to lift it up and down in the outlet channel. Since the vertical measurement pipes had a slight angle the aluminum piece that the SENSA sensor was fastened to would have to be bent with the same angle so the sensor would face the water flow straight on. This was supposed to be done in the field after measuring the angle. The angle turned out to be quite small, only 1.37°. It would be difficult to bend the aluminum piece so little, and it was decided to not bend the aluminum pieces.

Some changes to the frame were made after the sketch was delivered to the technicians. The place where the sensor would be fastened had to be moved 15cm from the perforated metal pipes. Figure 3.10 shows the final frame.

Figure 3.10: Finished measurement frame

3.3 Measurements

Student Vegard Ulvan joined the measurements at Ylja Power plant. His focus was to do a thermodynamic efficiency measurement. Trine Brath was in charge of measuring and finding the temperature and velocity distribution at the outlet, and Vegard Ulvan was in charge of the pressure measurements and in setting up the inlet probe.

3.3.1 Measurement procedure

The measurements were to be done over two days. There were some changes to the initial procedure (see chapter 3.4), but table 3.2 shows the final measurement procedure. The temperature was measured for 10 minutes at three locations across the channel

width, and at three different heights.

Measurement number	Number of injectors	Power [MW]	Distance from channel bottom [m]
1	1	5	0.7, 1.4, 2
2	1	8	0.7, 1.4, 2
3	1	10	0.7, 1.4, 2
4	2	12	0.7, 1.4, 2
5	2	16	0.7, 1.4, 2
6	2	20	0.7, 1.4, 2
7	3	18	0.7, 1.4, 3
8	3	22	0.7, 1.4, 3
9	3	28	0.7, 1.4, 3
10	4	24	1.4
11	4	28	1.4
12	4	33	1.4
13	4	36	1.4
14	6	34	0.7, 1.4, 2
15	6	40	0.7, 1.4, 2
16	6	46	0.7, 1.4, 2
17	6	50	0.7, 1.4, 2
18	6	55	1.4
19	6	60	1.4
20	6	65	1.4
21	6	40	1.4

Table 3.2: Final measurement procedure

The turbine runs mostly with 1, 2, 3 or 6 injectors. The combination with 4 or 5 injectors are rarely used. It was decided to only look at the temperature distribution for 1, 2, 3 and 6 injectors. Eidsiva wanted to know the efficiency for 4 injectors. The temperature and pressure was therefore measured for four different power settings using 4 injectors, but the temperature sensors in the outlet channel were kept at one constant elevation. Some additional measurements were done with 6 injectors at the power settings 55MW, 60MW and 65MW and 40MW (repeating point) to be able to make a better efficiency analysis.

3.3.2 Time Schedule

The measurements at Ylja hydropower plant took place between 9th of April and 13th of April.

Day 1: Drive to Ylja hydropower plant

Day 2: Rig up

Day 3: Measurements

Day 4: Measurements

Day 5: Rig down, and travel back to Trondheim

Eidsiva had given permission to use and control the hydropower plant from 09:00 until 21:00. due to changes in the measurement procedure (see chapter 3.4) it was possible to rig down on day 4 instead of day 5.

3.3.3 Rig up

The day of the rig up went as follows:

09^{00} – 10^{00}: Meeting with the three technicians that would help with rigging up the equipment. Did a risk assessment together.

10^{00} – 11^{30}: Unloaded all the equipment from the car. Inspected the measurement pipes. Inside all the holes there were burrs/sharp edges. Had to remove them to fit the Seabird SBE38 sensors.

11^{30} – 12^{30}: Lunch.

12^{30} – 13^{00}: Inspected the turbine buckets and injectors.

13^{00} – 14^{00}: Used a hole saw to remove the burrs/sharp edges around the holes in the pipes. Now the temperature sensors went in easily.

14^{00} – 15^{00}: Set up the vertical measurement.

15^{00} – 16^{30}: Tried to rig up the measurement frame with the SENSA RV2 sensors. The

frame was too long because the given distances between the vertical measurement pipes were too long. Ten centimeters of the main frame were cut off.

16^{30} – 17^{15}: Break.

17^{15} – 18^{00}: Rig up the measurement frame for the SENSA velocity sensors.

18^{00} – 19^{00}: Tried to get the voltage signal out of the turbine governor so that the exact generator power could be logged. Did not manage to get the signal.

Figure 3.11: Measurement pipes before and after using the hole saw.

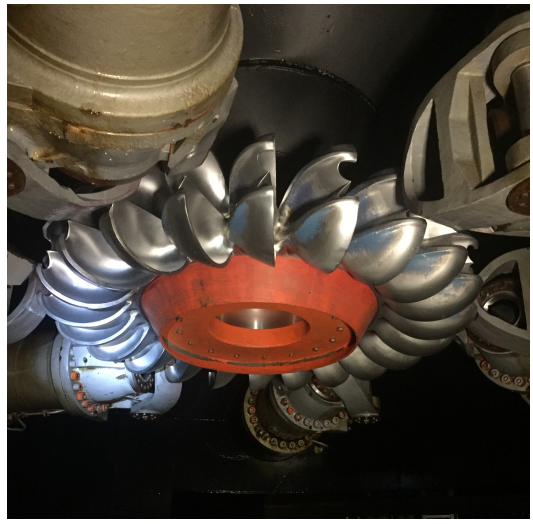

Figure 3.12: Pelton runner and injectors

3.3.4 Measurements

The measurements were done as described in the measurement procedure starting with measurements for 1 injector at 5MW. The measurements with 1, 2 and 3 injectors were done at day 3 from 09:00 until 20:30. The measurements with 4 and 6 injectors were done on day 4 from 09:00 until 15:00. The measurement conditions were good. It was sunny both days, and the temperature was around -4°. The stoplog was closed, meaning water from the streams were mixed in with the water from the reservoir, but this did not affect the measurements. Could see from the temperature measurements at the inlet that the inlet temperature was stable, and was around 1°C.

During the measurements Trine Brath was in charge of measuring the temperature, positioning the temperature sensors in the outlet channel, measuring the height of the water and controlling the turbine governor by setting the number of injectors and the power. The turbine governor chose which injector was to be used. In table 3.3 is an overview of which injector was running. The position of the injectors can be seen in figure 3.13. In addition to being manually controlled, the power was controlled by the frequency. The decision to leave the power frequency regulated was made by Eidsiva Energi. The frequency varied from minimum 49.92 to maximum 50.07 Hz, therefore the power also changed slightly. To try an stabilize the power the nozzle opening was set to not vary more than 20%.

Number of injectors	Which injector
1	5
1	2, 5
3	1, 3, 5
4	1, 2, 4, 5
6	1, 2, 3 ,4 ,5 ,6

Table 3.3: Injectors

The height of the water was measured using a laser distance measurer. It was difficult to get the correct distance because of the foam which formed in the upper layer of the channel flow. The distance was therefore measured several times to get an averaged value.

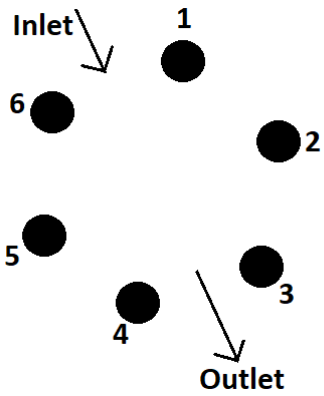

Figure 3.13: Position of injectors

Figure 3.14: Turbine shaft and injectors

The measurement points in the channel cross section can be seen in figure 3.15. The cross section is viewed with your back towards the turbine. Seabird sensor with ID=02 was used in the vertical pipe furthest to the left, ID=04 in the middle, and ID=05 to the right. There is only one measurement point (point 3) on the left side because the sensor got stuck in the pipe at this height.

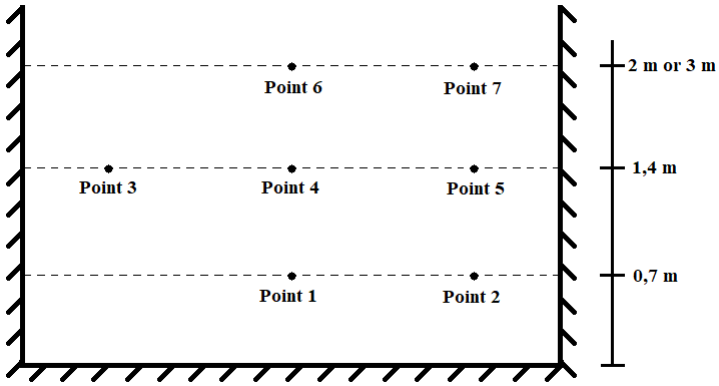

Figure 3.15: Measuring points at the outlet

The decision on what elevations to measure the temperature at was done in the field after seeing and measuring how high the water level was. The water level was 2.37 meters when running the turbine with 1 injector at the power 5MW. It was decided to measure the temperature at points 0.7 meter, 1.4 meter and 2 meters from the channel bottom. Continued to measure at 0.7 meters and 1.4 meters for the other power settings as well, and would change the position for measurement point 6 and 7 if the water level increased a lot. For measurements with 3 injectors the water level had increased with 1 meter compared to measurements with 1 injector and a decision was made to place measurement point 6 and 7 3 meters from the channel bottom instead of 2 meters. Went back to measuring at 2 meters, on the second day of measurements because the water level was not as high as it had been with 3 injectors the day before. In table 3.4 is the distance between the upper measurement point and the water surface. In hindsight the temperature could have been measured at 2.5 meters instead for 2 meters for the power settings 40MW, 46MW and 50MW.

# Injectors	Power settings	h_2
1	5MW	0.37m
1	8MW	0.37m
1	10MW	0.41m
2	12MW	0.40m
2	16MW	0.41m
2	20MW	0.46m
3	18MW	0.37m
3	22MW	0.33m
3	28MW	0.30m
6	34MW	0.66m
6	40MW	0.87m
6	46MW	1.07m
6	50MW	1.15m

Table 3.4: Height from temperature sensor to water surface, h_2

Figure 3.16: Temperature rig at the outlet

Vegard Ulvan did pressure measurements every time the temperature sensors were located 1.4meter from the channel bottom.

3.3.5 Rig down

The measurements took less time than anticipated. They were done before 16:00 on day 4. Used approximately 2 hours to rig down. Everything went according to plan. The only challenge was the Seabird SBE38 sensor that was stuck in the measurement pipe. It made dismantling the measurement pipes a little bit more difficult, but the technicians from Eidsiva managed to do it and got the sensor undamaged out of the pipe.

3.4 Changes

During planning of the measurements and the rig up several changes had to be made to the measurement procedure for different reasons.

Different cross-sections

During the excursion til Ylja hydropower plant in February it was discovered that it was not possible to measure the cross sectional energy at different distances from the turbine center. This was due to the fact that the outlet channel goes straight into the lower reservoir. Draining the outlet channel would require to much resources and time. Without draining the outlet channel it would not be possible to move a measurement frame further away from the turbine center. The objective of this thesis did therefore change. The new objective was to find the energy distribution in one cross section when running different types of combinations of injectors.
The initial measurement procedure was as follows:

1. Run all the 6 injectors individually at power settings 5MW, 8 MW and 10 MW. 9 measurement points.

2. Run 3 injectors at the same time. Run number 1, 3 and 5 together. And then

number 2, 4 and 6 together. Run at the power settings 18MW, 22MW, 28MW. 9 measurement points.

3. Run all 6 injectors at the same time at the power settings 34MW, 40MW, 46MW. 9 measurement points.

4. If there is time to spare: Run 2 injectors at 12MW, 16MW and 20 MW. Run 4 injectors at 24MW, 28MW and 32MW. Run 5 injectors at 28 MW, 34MW and 40 MW.

Controlling the injectors

At the day of the rig up it was discovered that it was not possible to specify which injector would be running. It was only possible to decide how many injectors would be running. The reason for this was the deflector. It is normal for the injectors and the deflector to have two separate servomotors, but at Ylja hydropower plant they shared one. This is an old system, and it means that the deflector decides the opening of the nozzles.

Problems with the velocity sensors

Before putting the frame with the SENSA RV2 sensors into the water, the sensors were tested to see if they and the LabVIEW program worked. All the sensors and the Aqua Data RMX worked. After putting the sensors in the water another measurement test was done. This time the Aqua Data RMX, which shows the velocities measured by the sensors, showed random symbols and numbers, as seen in figure 3.17. After turning it off and on, changing the batteries and changing the sensors it was concluded that there was something wrong with either the sensors or with the Aqua Data RMX. It was no longer possible to do velocity measurements. The frame with the sensors was removed from the channel. Back at the Water Power Laboratory at NTNU the sensors were tested again, and they worked. One reason for why they did not work might have been because there were disturbances from the other electrical equipment which produced large electromagnetic fields, such as the generator.

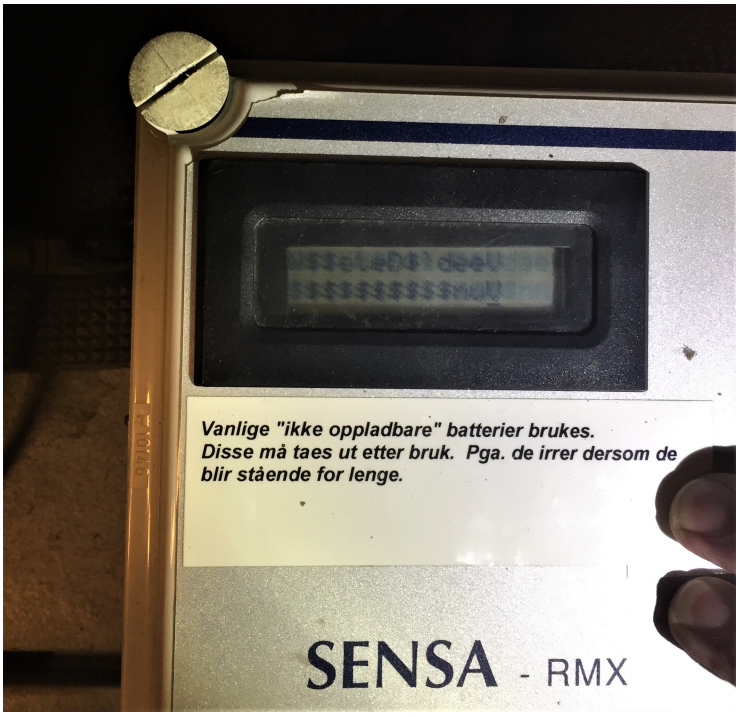

Figure 3.17: Picture of the Aqua Data RMX box when it did not work.

Fewer measurement points

The original plan was to have 9 (3x3) measurement points. When putting the temperature sensors into the pipes one of them got stuck at 1.4 meter above the channel bottom. It was not possible to move it up or down. Had tested the day before if the Seabird SBE38 sensors fit the pipes, and they all did, but as mentioned earlier with little clearance. The metal pipes had been standing in the cold water over night, and the pipe might have shrunk a little bit. Enough to make the inner diameter of the pipe too small for the Seabird SBE38 sensor. There were no difficulties with the other two sensors. The temperature was therefore measured in 7 measurement points instead of the intended 9.

Chapter 4

Results

4.1 Temperature

The some of the measured temperatures can be found in figure 4.1, 4.2,4.3,4.4, 4.5 and 4.6. The rest of the temperatures were also plotted and can be found in appendix E. ID=01 is the sensor which measured the inlet temperature, ID=02, ID=04 and ID=05 measured the outlet temperature.

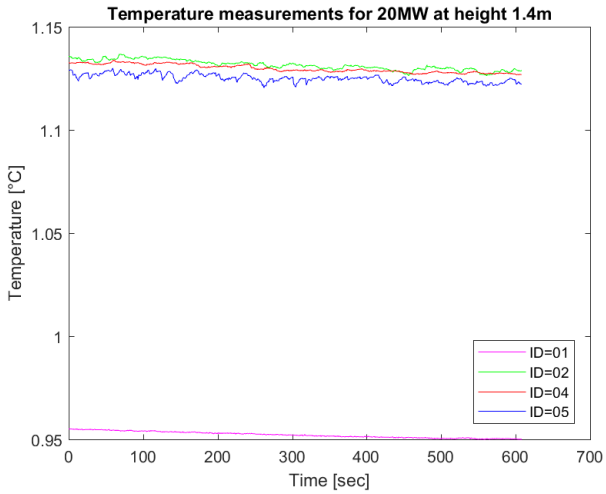

Figure 4.1: Temperature measurements: 2 injector, 20MW, h=1,4m

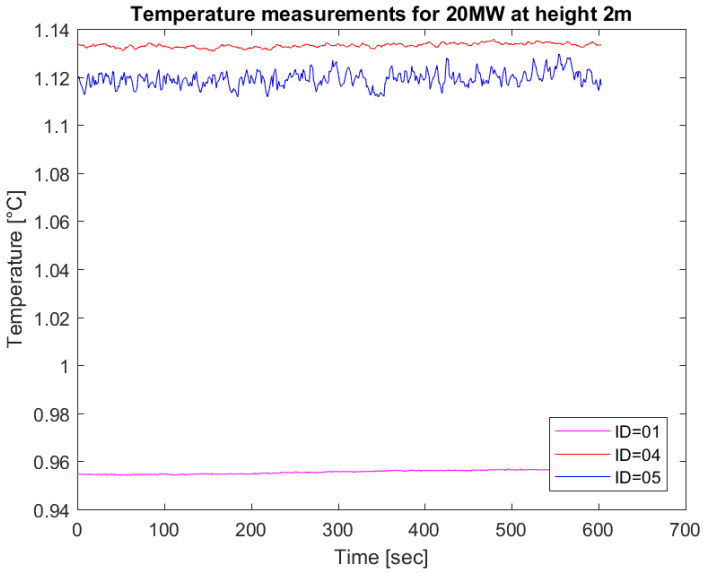

Figure 4.2: Temperature measurements: 2 injector, 20MW, h=2m

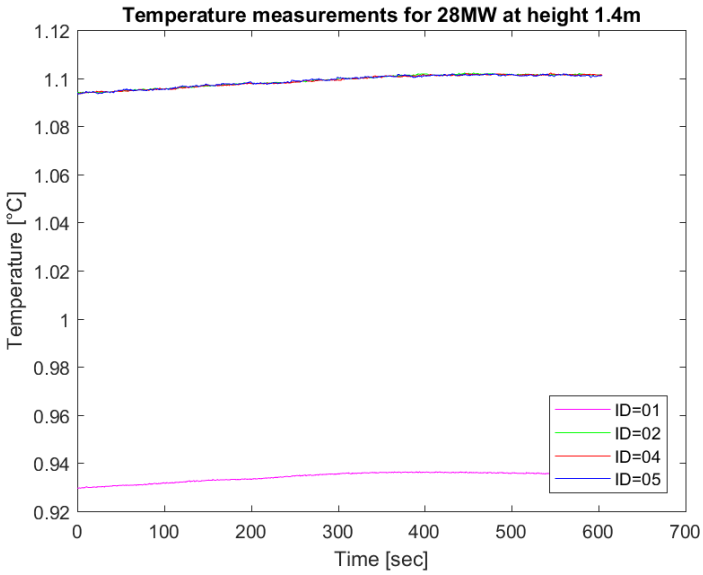

Figure 4.3: Temperature measurements: 3 injector, 28MW, h=1,4m

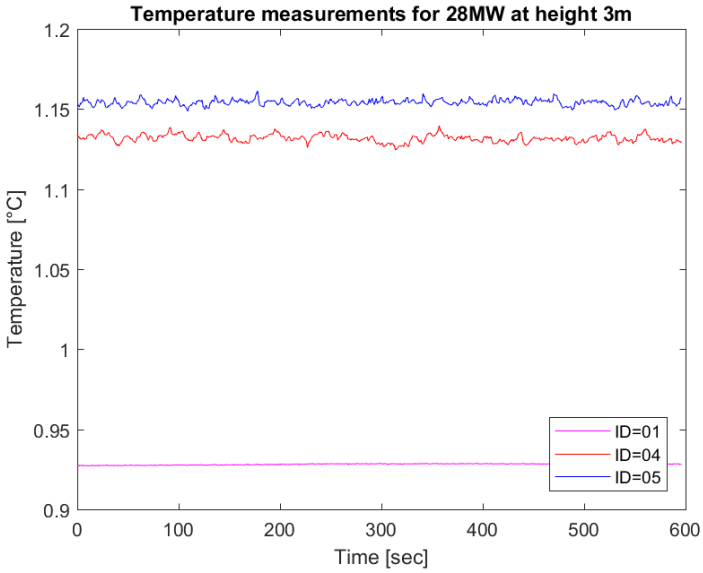

Figure 4.4: Temperature measurements: 3 injector, 28MW, h=3m

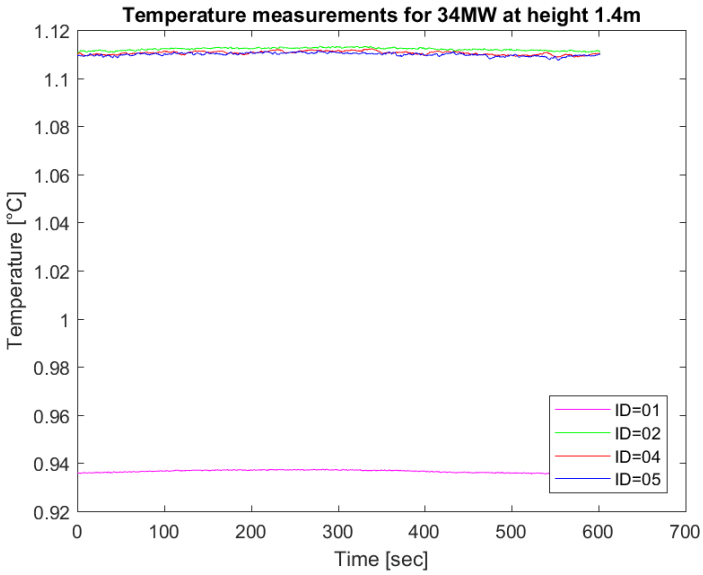

Figure 4.5: Temperature measurements: 6 injector, 34MW, h=1,4m

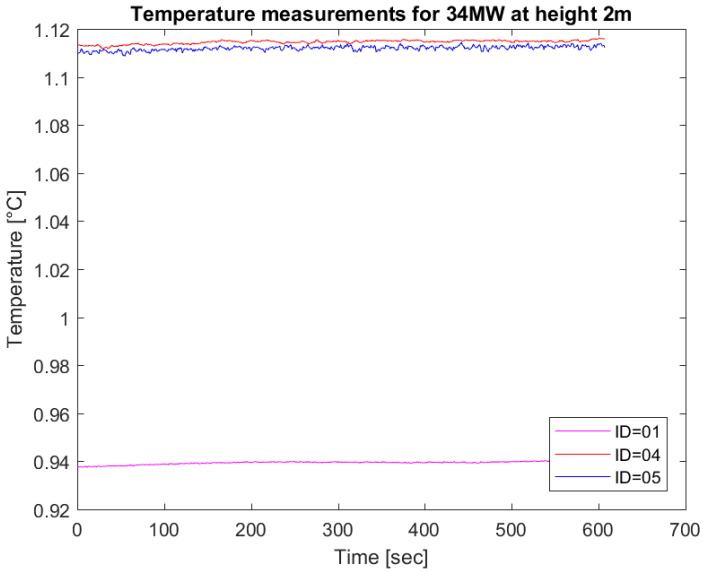

Figure 4.6: Temperature measurements: 6 injector, 34MW, h=2m

4.2 Thermal energy distribution

After finding the temperature at the inlet and outlet the thermal energy was calculated. Figure 4.7 to 4.19 shows the thermal energy in the cross section. In the figures, the thermal energy is shown as a positive value, but when calculating the mechanical energy the thermal energy is negative. This is because the outlet temperature is larger than the inlet temperature.

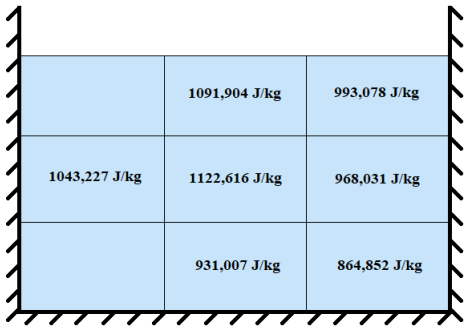

Figure 4.7: Thermal energy for 5MW (1 injector)

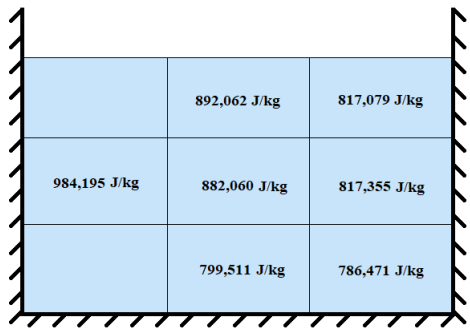

Figure 4.8: Thermal energy for 8MW (1 injector)

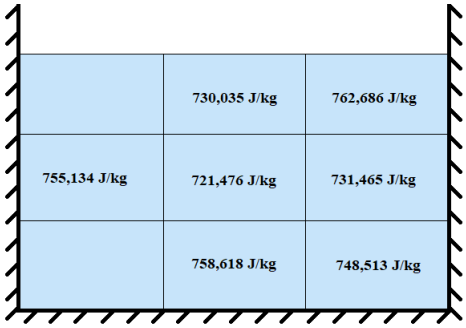

Figure 4.9: Thermal energy for 10MW (1 injector)

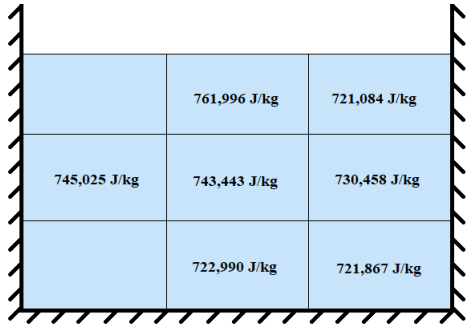

Figure 4.10: Thermal energy for 12MW (2 injectors)

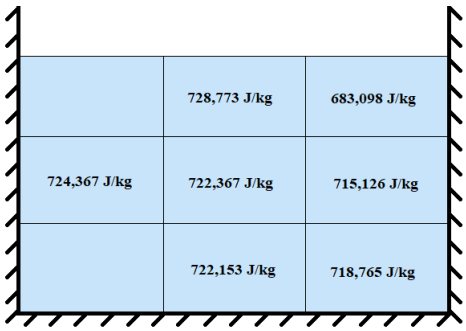

Figure 4.11: Thermal energy for 16MW (2 injectors)

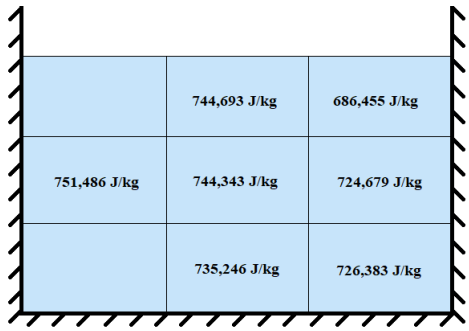

Figure 4.12: Thermal energy for 20MW (2 injectors)

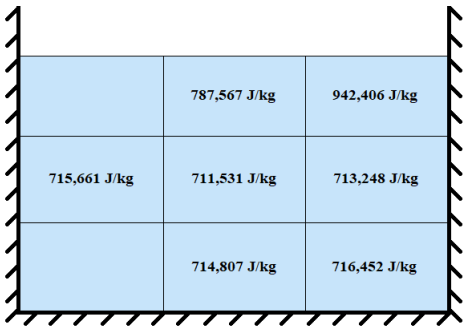

Figure 4.13: Thermal energy for 18MW (3 injectors)

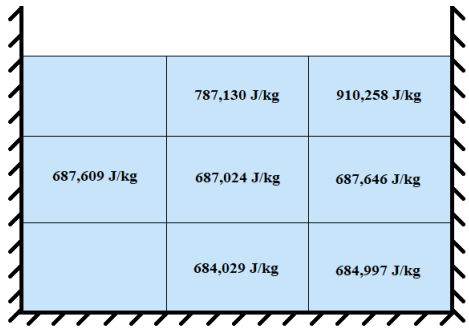

Figure 4.14: Thermal energy for 22MW (3 injectors)

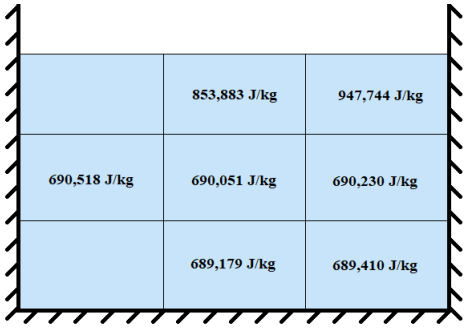

Figure 4.15: Thermal energy for 28MW (3 injectors)

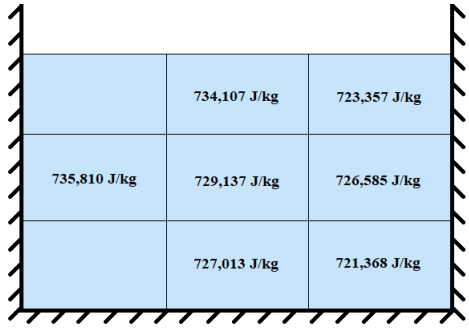

Figure 4.16: Thermal energy for 34MW (6 injectors)

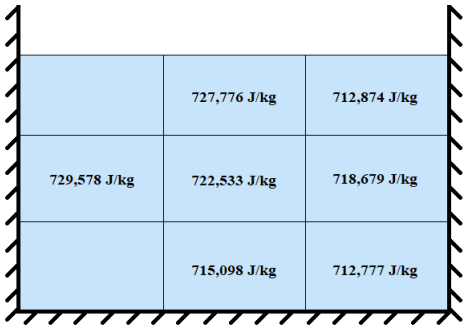

Figure 4.17: Thermal energy for 40MW (6 injectors)

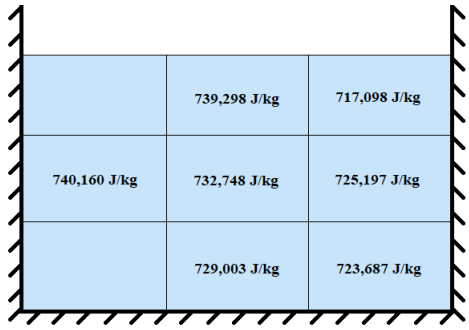

Figure 4.18: Thermal energy for 46MW (6 injectors)

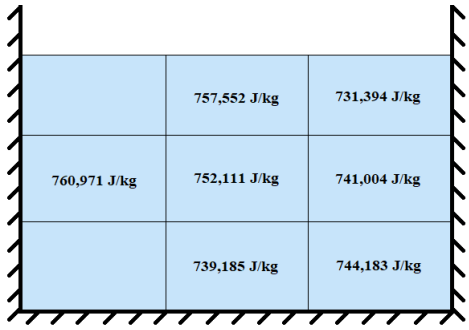

Figure 4.19: Thermal energy for 50MW (6 injectors)

4.3 Uncertainty

It is interesting to see how big the uncertainty of the thermal energy is compared to the pressure energy, potential energy and kinetic energy. To find the uncertainty the mechanical and hydraulic energy had to be calculated. The mechanical and hydraulic energy was calculated using equations 2.2 and 2.3. The pressure values were taken from Vegard Ulvan measurements [12].

The mechanical kinetic energy was set to be zero because the velocity c_{1-1} was set to be zero. The design of the probe where the inlet pressure and the inlet temperature were measured, made it so that the stagnation pressure was measured. The water level in the measurement probe is almost equal to the pressure height plus velocity height. By letting the height in the probe represent the pressure height, the velocity height will be included. The velocity c_{1-1} is therefore included in the pressure p_{1-1}. The hydraulic kinetic energy was found by using the turbine power and the volume flow rate (see appendix D).

IEC 41 gives some corrections for the mechanical energy. These corrections are not always necessary, either because the correction conditions do not occur or they are of such a size that they won't make an impact on the calculations. These corrections are:

- Mechanical energy slit water (only for Francis turbines): not included.
- Temperature variation inlet: not included because the temperature was almost stable.
- Heating between the air in the hydropower plant and the water: not included.
- Direct heat dissipation the air in the hydropower plant and the water: not included.

After calculating the mechanical and hydraulic energy the uncertainty of the calculation was calculated. The uncertainty was found using the equations in appendix D. Some uncertainties are given by IEC 41, or come from calibration of the equipment, and some had to be assumed. Tables D.1, D.2 and D.3 in appendix D shows the uncertainties used to calculate the total uncertainty.

The uncertainty in the mechanical pressure energy, mechanical kinetic energy, mechanical potential energy and the mechanical thermal energy for the different measurement point at power settings 5MW, 20MW, 28MW and 34MW are found in table 4.1, 4.2, 4.3 and 4.4. Similar tables for the rest of the power settings are found in appendix F.

Measurement point	$e_{Em,pressure}$ $[J/kg]$	$e_{Em,kinetic}$ $[J/kg]$	$e_{Em,potential}$ $[J/kg]$	$e_{Em,thermal}$ $[J/kg]$	$e_{Em,total}$ $[J/kg]$
1	13,4751	0	1,3886	37,4054	39,7827
2	13,4741	0	1,3886	37,7730	40,1283
3	13,4905	0	1,3886	36,7915	39,2114
4	13,4917	0	1,3886	36,3640	38,8109
5	13,4894	0	1,3886	37,2020	39,5964
6	13,5031	0	1,3886	36,5292	38,9697
7	13,5016	0	1,3886	37,0652	39,4722

Table 4.1: Uncertainty in mechanical energy for turbine power P_t =5MW

Measurement point	$e_{Em,pressure}$ $[J/kg]$	$e_{Em,kinetic}$ $[J/kg]$	$e_{Em,potential}$ $[J/kg]$	$e_{Em,thermal}$ $[J/kg]$	$e_{Em,total}$ $[J/kg]$
1	13,4512	0	1,3886	38,4436	40,7526
2	13,4511	0	1,3886	38,4941	40,8002
3	13,4652	0	1,3886	38,3518	40,6707
4	13,4652	0	1,3886	38,3924	40,7089
5	13,4649	0	1,3886	38,5045	40,8145
6	13,4770	0	1,3886	38,3910	40,7115
7	13,4762	0	1,3886	38,7237	41,0251

Table 4.2: Uncertainty in mechanical energy for turbine power P_t =20MW

Measurement point	$e_{Em,pressure}$ $[J/kg]$	$e_{Em,kinetic}$ $[J/kg]$	$e_{Em,potential}$ $[J/kg]$	$e_{Em,thermal}$ $[J/kg]$	$e_{Em,total}$ $[J/kg]$
1	13,3846	0	1,3886	38,4982	40,7823
2	13,3847	0	1,3886	38,4969	40,7810
3	13,3985	0	1,3886	38,4913	40,7802
4	13,3985	0	1,3886	38,4939	40,7827
5	13,3985	0	1,3886	38,4929	40,7818
6	13,4324	0	1,3886	37,5679	39,9212
7	13,4338	0	1,3886	37,0470	39,4319

Table 4.3: Uncertainty in mechanical energy for turbine power P_t =28MW

Measurement point	$e_{Em,pressure}$ $[J/kg]$	$e_{Em,kinetic}$ $[J/kg]$	$e_{Em,potential}$ $[J/kg]$	$e_{Em,thermal}$ $[J/kg]$	$e_{Em,total}$ $[J/kg]$
1	13,3586	0	1,3886	38,1966	40,4890
2	13,3585	0	1,3886	38,2288	40,5193
3	13,3725	0	1,3886	38,1471	40,4470
4	13,3724	0	1,3886	38,1851	40,4828
5	13,3723	0	1,3886	38,1997	40,4964
6	13,3843	0	1,3886	38,1574	40,4606
7	13,3842	0	1,3886	38,2186	40,5183

Table 4.4: Uncertainty in mechanical energy for turbine power P_t =34MW

The uncertainty shown in tables 4.1, 4.2, 4.3 and 4.4 consists of the systematic and random uncertainty. For the uncertainty in the thermal energy the systematic uncertainty gives the biggest contribution. The uncertainty in the heat capacity, e_{cp} and the uncertainties related to faulty exploration of the energy distribution, $e_{E_{10}}$ and $e_{E_{20}}$ are very large. The random uncertainty was very small, between 10^{-4} and 10^{-5}.

4.4 Efficiency curves

The result from the thermodynamic efficiency analysis is given in figure 4.20. The graph was made by Vegard Ulvan and more about the the efficiency is written in his master thesis "Pressure pulsations and efficiency measurements at Smeland Power Plant" [12].

The thermodynamic measurements made by E-CO in 2008 concluded that there had been a significant decrease in efficiency with 6 needles since Kværnes measurements in 1985. The measurements taken in 2018 showed that this was not the case, and when comparing the measurements in 1985 and 2008 it could be seen that their uncertainties overlap.

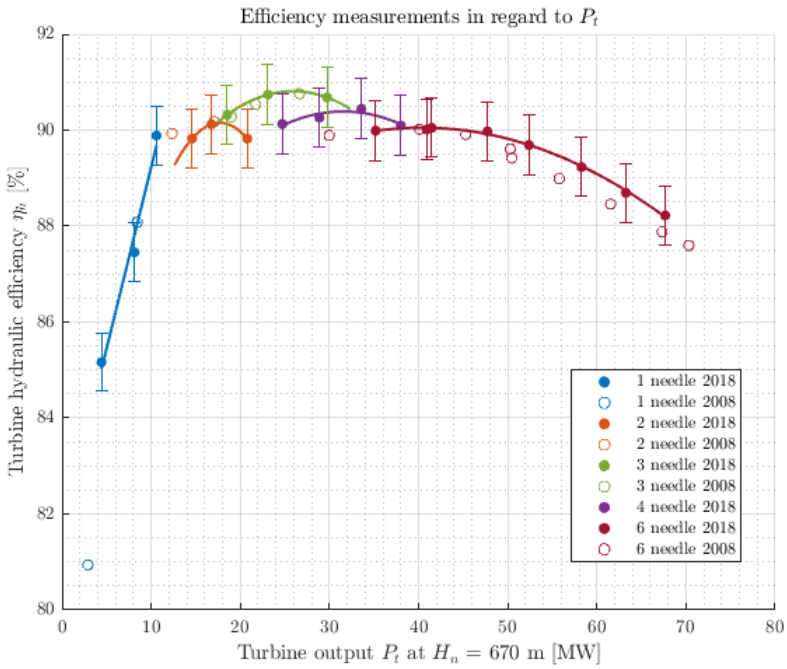

Figure 4.20: Efficiency measurements in regard to P_t

Chapter 5

Discussion

5.1 Thermal energy

The results of the measurements shows that the thermal energy is not the same across the cross sections. Some areas have higher thermal energy than others. This confirms that the energy in the outlet channel close to the Pelton turbine is not homogeneous.

It is a bit difficult to find a repeating pattern on how the temperature behaves in the outlet. It is also difficult to get the complete picture of the thermal energy distribution in the cross sections since the temperature in the left side of the channel was only measured at one height.

Some patterns can be seen. For all the power settings, except for 10MW, the thermal energy in the middle of the cross section (measurement point 1, 4 and 6) rises with distance from the bottom. There is no clear pattern for the area closest to the right wall, measurement point 2, 5 and 7. The thermal energy here sometimes increases with distance from the channel bottom, and sometimes decreases. It's not possible to make any conclusions about the energy distribution in the area closest to the left wall since there was only one measurement point there.

Another observation is that for measurements with 1, 2 and 6 injectors the thermal

energy was lower closer to the right wall than in the middle. For 3 injectors the water close to the right wall is warmer than the water in the middle. This can be because the water is mixed differently when there are three water jets which hits the Pelton buckets. The difference in thermal energy can also be seen from the temperature plots, figure 4.1 to 4.6. Temperature plots for other power settings can be found in appendix E. For 1, 2 and 6 injectors the temperature plots shows that sensor ID=05, which measured point 2, 5 and 7, measures a lower temperature than sensor ID=04, which measured point 1, 4 and 6. For 3 injectors it is the opposite.

The temperature plots and figures 4.7 to 4.19 also shows that with increased power the temperature at height 0,7 meters and 1,4 meters from the channel bottom becomes more stable, and the thermal energy is approximately the same across the width. This means that when the power, and thereby the volume flow rate, is increased the water in these areas are more mixed. When doing a thermodynamic efficiency measurement a horizontal "sampling beam" is often used. The sampling beam measures the average temperature over the channel width. If the temperature over the channel width are approximately the same the measured mean temperature is very representative of the temperature of the water. What can be seen from the measurements is that the temperature measured in the upper layer of the flow, at height 2 or 3 meter from the channel bottom, is more unstable and it is not constant across the channel width. The temperature differences across the channel width is larger than for the lower layer flow. In the upper layer of the flow air is mixed in with the water. Since the entrained air is warmer than the water heat exchanging will occur and the water temperature will increase. The mixing of air and water could be seen in observations of the flow, and in the measurements. The mixing of air and water in the upper layer gives a wrong representation of what the water temperature actually is. How large the area with entrained air is difficult to say. It changes with the volume flow rate and across the width of the channel.

The temperature was measured only 2.5 runner diameters from the turbine, which is not in compliance with IEC 41. IEC 41 requires that temperature measurements are done 4 to 10 runner diameters for the reason that in this area the water is more mixed.

The power of entrained air is seen especially well with the thermal energy distribution for the power settings 18MW, 22MW an 28MW. For these power settings the temperature was measured at 3 meters instead of 2 meters as the rest. Especially measurement point 7 measured a much higher thermal energy than the rest.

Since different areas in the cross sections have different values of thermal energy it is important to know how much weight to put on each temperature measurements. Some places it might be correct to take the mean value of the temperature, but other places, especially in the upper layer, it will not be correct. In order to achieve the most correct average energy in the outlet channel, the measured water should be weighted proportionally with flow rate in the measurement point. When using a "sampling beam" to measure the temperature the water measured in one place in the cross section may encounter greater resistance than water elsewhere in the cross section because the flow path to the thermometer is longer. If the temperature at this point is higher than other places this temperature will be weighted too little and the resulting average temperature will be too small. When the temperature measured is too small the thermal energy will be too small and the efficiency too high. It is therefore important to also measure the velocity in the outlet. Would have been interesting to measure the velocity and calculate the difference in efficiency with weighted and unweighted temperature measurements.

Can argue that if only the temperature in the area where the air and water is not mixed is measured the averaged temperature and the efficiency calculations will be more correct since the waters temperature will not have been influenced by the air. It is difficult to know exactly where the air and water stops mixing. The depth of the mixed layer changes with increased flow. It will therefore be difficult to know for certain that the measurements are done in an area without entrained air. To only measure the temperature in the lower layer of the flow will also give a wrong representation of the energy in the water. The measurements would then not show the whole picture of the temperature distributions in the water.

5.2 Uncertainty

The uncertainty analysis showed that the thermal energy has the largest uncertainty, as seen in tables 4.1, 4.2, 4.3 and 4.4 and the tables in appendix F.

The uncertainties are approximately the same for all the measurements, the small variations in the uncertainties comes from the difference in measured temperature. The result from uncertainty analysis tells us that it is important to measure the temperature accurately. A large part of the uncertainty in the thermal energy comes from the uncertainty related to the heat capacity. This uncertainty is difficult to make smaller because it comes from the uncertainty in the values given in a table with heat capacity values. Other contributors to the large uncertainty are related to faulty exploration of the energy distribution. These two uncertainties, $e_{E_{10}}$ and $e_{E_{20}}$, have to be added when the velocity is not measured. $e_{E_{20}}$ is very large because it is 0,6% of the mechanical energy. Usually the velocity is not measured when doing a thermodynamic efficiency measurement, and the temperature from different places in cross section are equally weighted when calculating the efficiency. Without the velocity measurements to weigh the temperature values the the efficiency measurement will have a large uncertainty.

Chapter 6

Conclusion

6.1 Conclusion

The field measurements confirmed that the thermal energy in the outlet cross section is not homogeneous. Some pattern for how the energy behaves in the cross section can be seen, but it varies with the number of injectors running. Especially 3 injectors stands out from the rest. In the top layer of the flow air was entrained in the water. This gives inaccurate temperature measurements for the top layer, since the airs temperature is warmer than the waters. The thermal energy in this area varied a lot from the rest of the cross sectional area. There is also not enough data on what happens on the left side of the channel to say how the energy distribution is there. Can therefore not conclude that the energy distribution in a cross section always behaves in a certain pattern.

The inhomogeneous energy distribution makes it important to know how much weight to put on each temperature measurements. Weighting all the temperature measurements the same when calculating the thermodynamic efficiency will give incorrect efficiency. By weighting the temperature measurements wrongly the thermal energy might be higher or lower than it really is. Too large thermal energy will give too small efficiency, and too small thermal energy will give too high efficiency.

The uncertainty analysis for thermodynamic efficiency measurements showed that the largest uncertainty is given by the thermal energy measurements. One of the largest contributor to this uncertainty was the faulty exploration of the energy distribution, which comes from not knowing how to weight the temperature measurements. This uncertainty can be minimized by measuring the velocity, because the velocity distribution gives information on how much weight to put on the temperature measurements in different parts of the cross section.

6.2 Further work

For further work finding another power plant with a Pelton turbine where it is possible to measure at different distances from the turbine outlet is desirable, or a power plant where it is possible to locally decide which injector is running. When measuring the velocity a propeller current meter should be used instead of a magnetic flow meter. New temperature measurements can also be done with maybe even more measuring points, and extra care should be taken so that none of the temperature sensors get stuck in the measuring pipes.

It might also be an idea to measure the amount of air in the water. Then it would be possible to make conclusions on how the temperature of the air influences the waters temperature.

Bibliography

[1] Akinlade, O. G *Effects of surface roughness on the flow characteristic in a turbulent boundary layer.* Thesis. University of Saskatchewan. 2005

[2] Bonakdari H., Larrarte F., Lassabtere L., Johannis C. *Turbulent velocity profile in fully-developed open channel flows.* Springer. 2007

[3] Brath T. *Energy measurement in a free surface channel* Project thesis. NTNU. 2018

[4] Brennen Prof. C. E. *Internet book on Fluid dynamics*
Retrieved from URL `http://brennen.caltech.edu/fluidbook/` at 03.11.2017.

[5] Bryhni T., Dahlhaug O. G, Hulaas H. *Multipoint Thermodynamic Measurements - A Statistical Approach to Uncertainty Levels* IGHEM Conference, 2000.

[6] Bøkko E. Hulaas H., Nilsen E, Vinnogg L. *Thermodynamic Efficiency Measurements of Pelton Turbines. Experience from Investigation of Energy / Temperature Distribution in the Discharge Canal Measuring Section.* The 7th In ternational Conference on Hydraulic Efficiency Measurements, September 2008

[7] Chauhdry M. H. *Open-Channel Flow.* Springer. 2nd Edition. 2008

[8] Doeblin E. O. *Measurement systems: Application and design.* McGraw-Hill Education. 4th edition. 1990

[9] Høydal A. *Virkningsgradmålinger av en høytrykks Pelton (Francis) turbin* Masterthesis. NTNU. 2011

[10] IEC 41. *Field acceptance tests to determine the hydraulic performance of hydraulic performance of hydraulic turbines, storage pumps and pump turbines*. International Standard. Geneva, Switzerland. 1991

[11] Kjølle Prof A. *Hydraulisk måleteknikk. Grunnleggende prinsipper og målemetoder*. Trondheim. 2003

[12] Kverno J., Ulvan V. *Pressure pulsations and efficiency measurements at Smeland Power Plant* Master thesis. NTNU. 2018

[13] Nilsen E. *Virkningsgradmåling på vannturbin*. Masterthesis. NTNU. 1991

[14] Nordby O. A., Tech. rep., OAN AS. *Configuration and calibration manual*. 2003

[15] Oppland Energi AS *Information about Ylja hydropower plant* Retrieved from URL `http://www.opplandenergi.no/Kraftverksoversikt/Ylja/` at 15.05.2018.

[16] Ramdal J. *Efficiency measurements in low head hydro power plants*. Doctoral thesis. NTNU. 2011

[17] Solemslie B. W. *Compendium in Instrumentation, Calibration and Uncertainty Analysis* NTNU.

[18] Solvik S. G. *Efficiency- and Pressure pulsation measurements at a low head hydro power plant* Masterthesis. NTNU. 2016

[19] White F. M. *Viscous Fluid Flow*. McGraw-Hill Education. 3rd edition. 2006

[20] Aqua-Data Services Ltd *Information sheet about SENSA RMX*

Appendix A

Sketch of velocity measurement frame

Hovedramme sett ovenifra

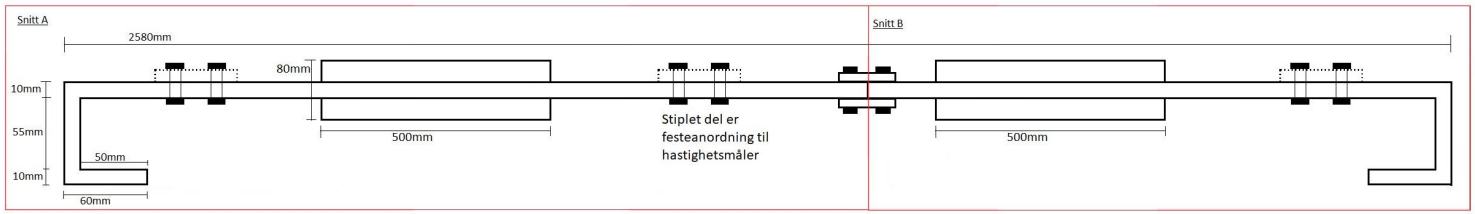

SNITT A

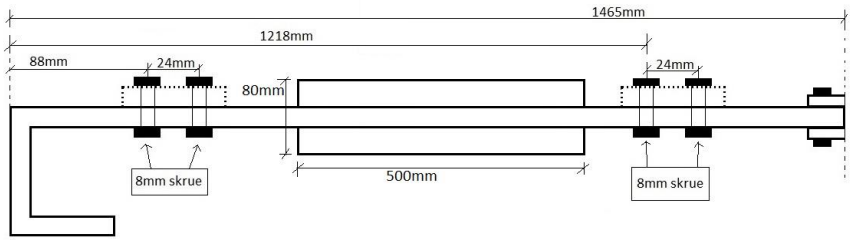

SNITT B

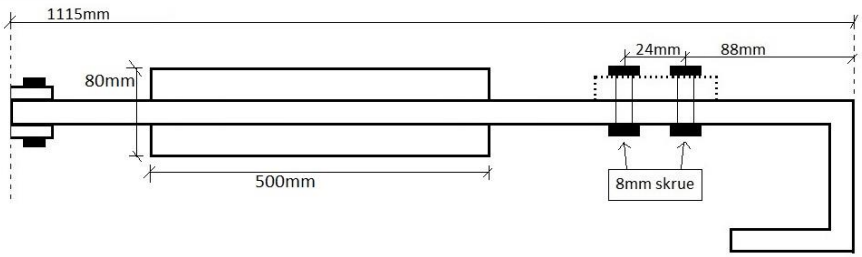

Hovedramme sett foran i fra

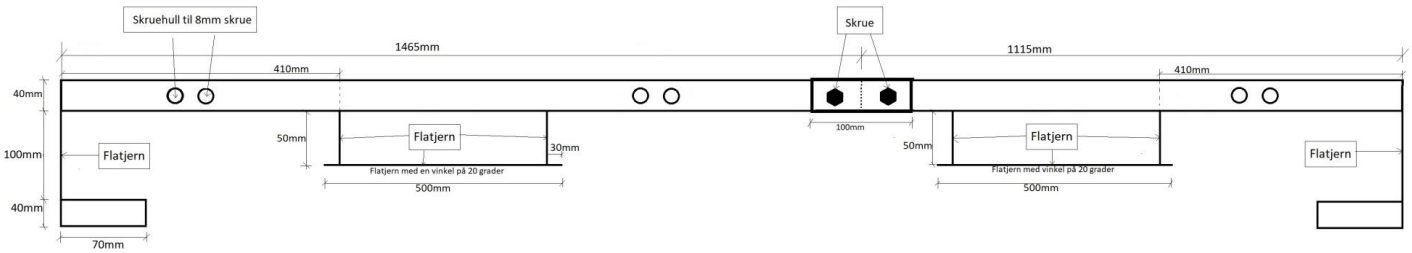

A3

Flatjern - til å presse hovedramma ned
Sett fra siden

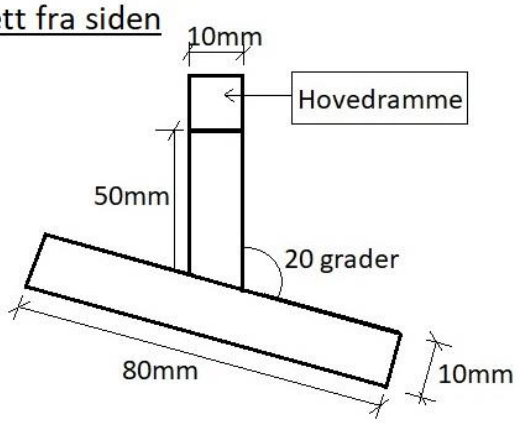

Hovedramme - sett fra siden

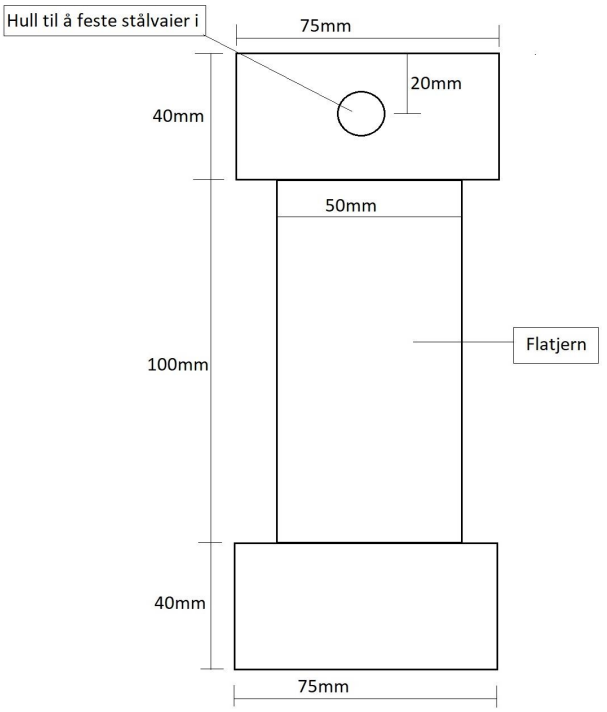

Feste hastighetssensorer - 3 stk.

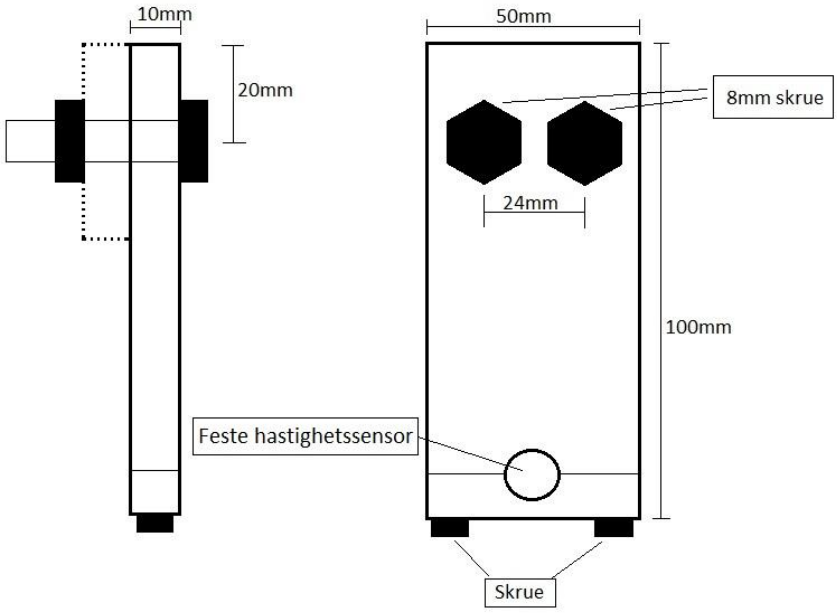

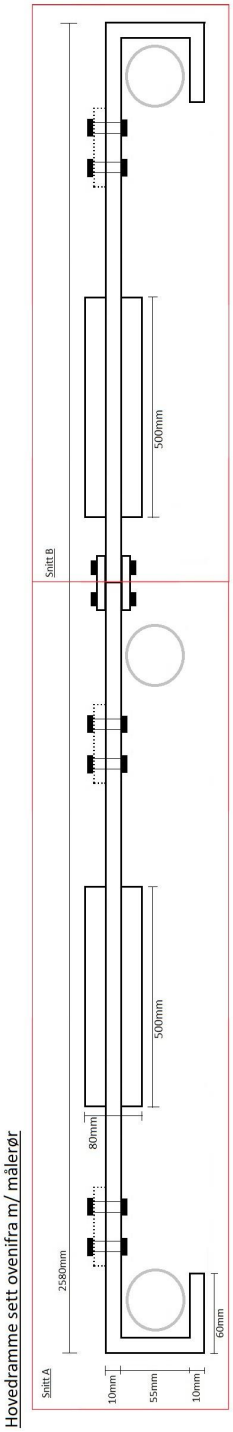
Hovedramme sett ovenifra m/ målerør
Snitt A
Snitt B
2580mm
80mm
500mm
500mm
10mm
55mm
10mm
60mm

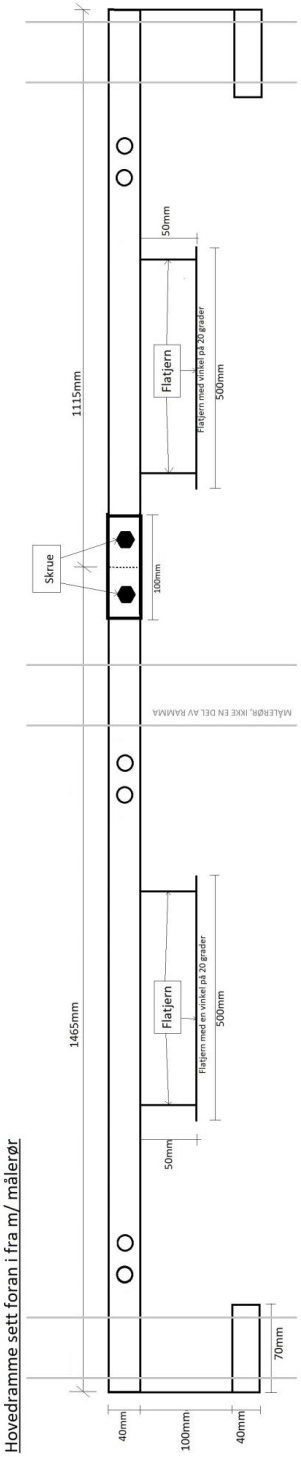
Hovedramme sett foran i fra m/ målerør
1115mm
1465mm
Skrue
100mm
50mm
Flatjern
Flatjern med vinkel på 20 grader
500mm
50mm
Flatjern
Flatjern med en vinkel på 20 grader
500mm
70mm
40mm
100mm
40mm

Appendix B

LabVIEW program for velocity measurements

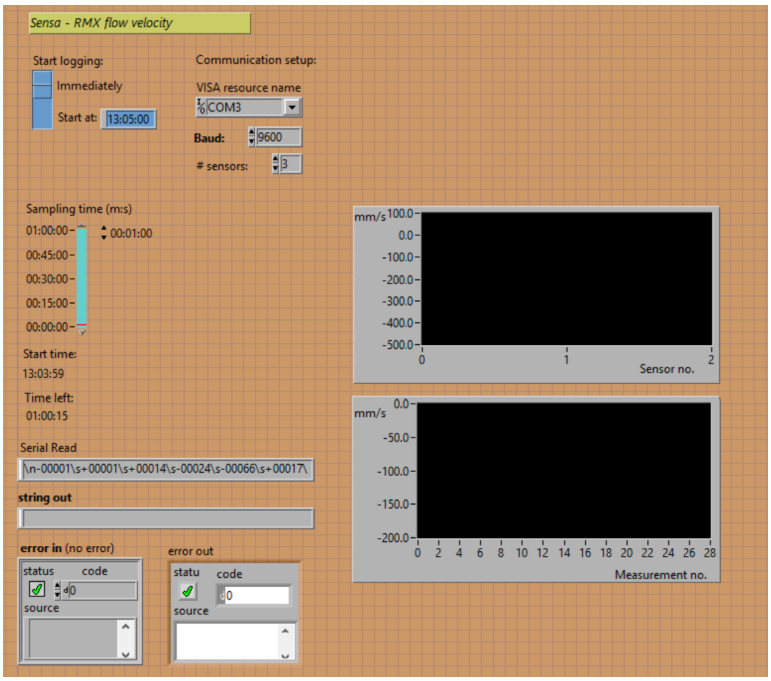

Figure B.1: LabVIEW, SENSA RV2 sensor program, Front panel

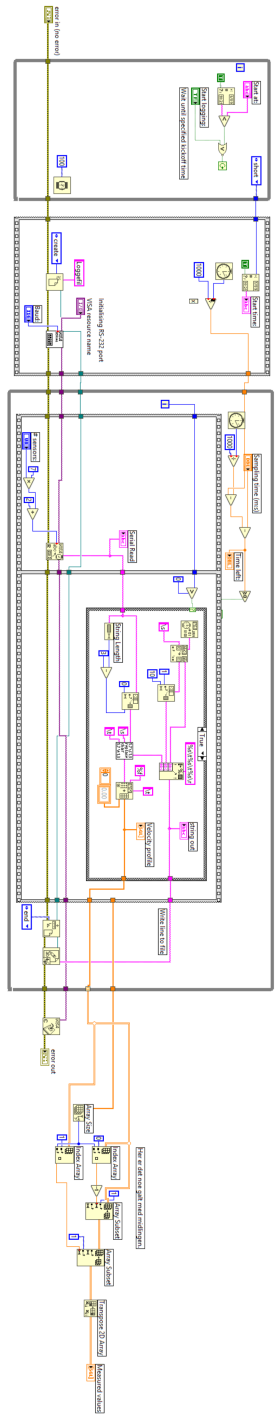

Figure B.2: LabVIEW, SENSA RV2 sensor program, Block diagram

Appendix C

LabVIEW program for temperature measurements

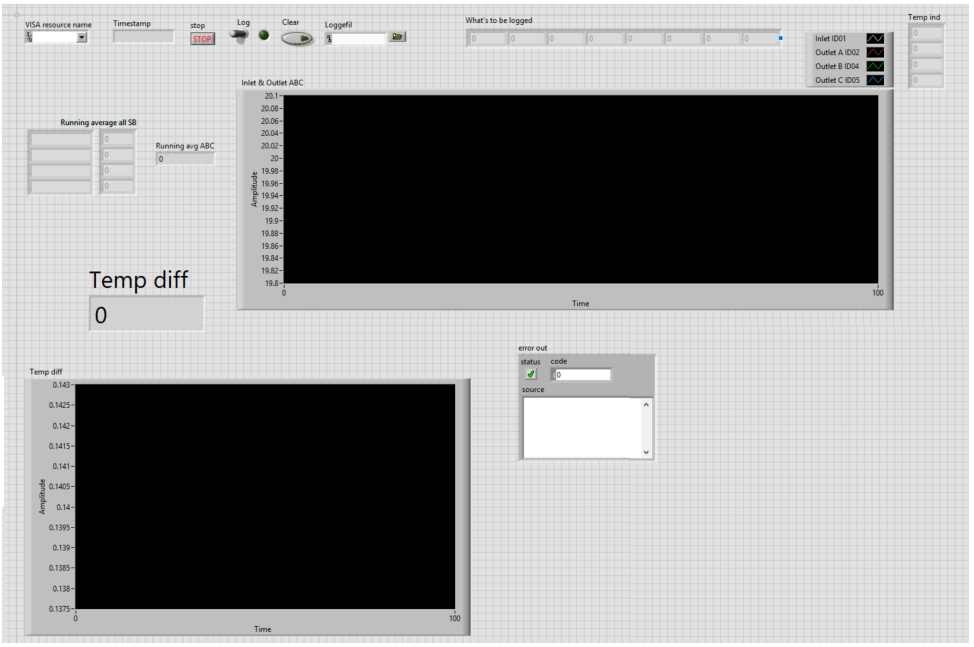

Figure C.1: LabVIEW, Seabird SBE38 program, Front panel

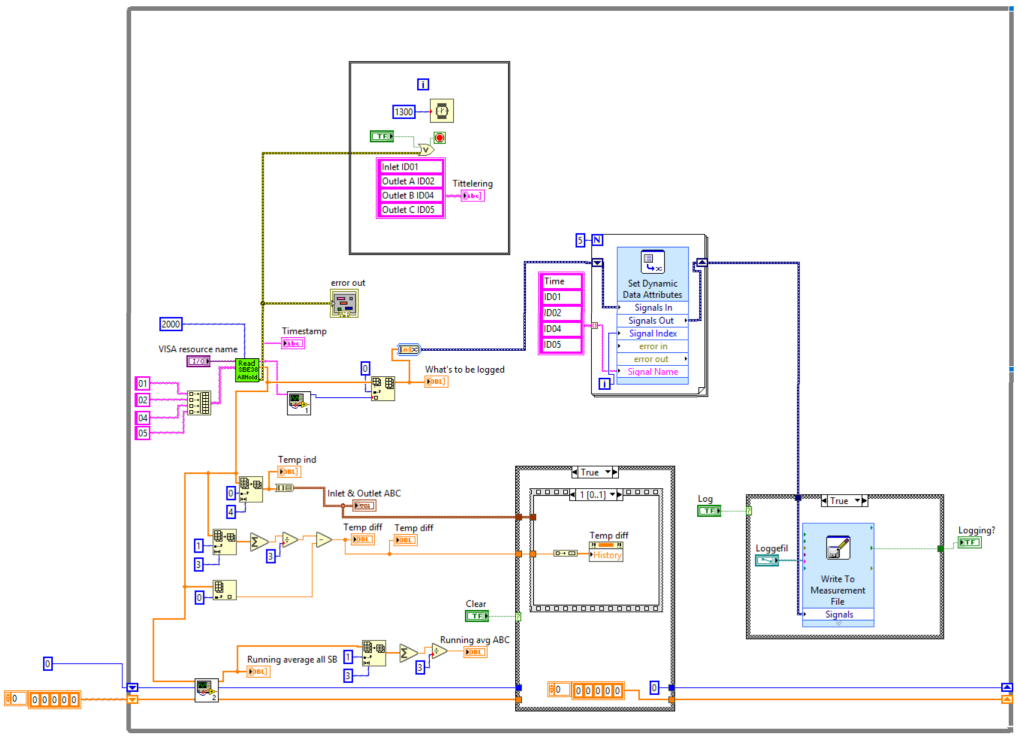

Figure C.2: LabVIEW, Seabird SBE38 program, Block diagram

Appendix D

Uncertainty analysis

D.1 Total uncertainty

The total uncertainty of the thermodynamic efficiency consists of a systematic uncertainty and a random uncertainty.

$$f_{tot} = \pm\sqrt{f_s^2 + f_r^2} \tag{D.1}$$

The systematic uncertainty is given by:

$$f_s = \pm\sqrt{f_{E_{m_s}}^2 + f_{E_{h_s}}^2} \tag{D.2}$$

The random uncertainty is given by:

$$f_r = \pm\sqrt{f_{E_{m_r}}^2 + f_{E_{h_r}}^2} \tag{D.3}$$

D.2 Systematic uncertainty

D.2.1 Mechanical energy

In this section the systematic mechanical energy uncertainty will be derived.

The mechanical energy is given by equation:

$$E_m = E_{m,pressure} + E_{m,kinetic} + E_{m,potential} + E_{m,thermal} + \delta E_m \tag{D.4}$$

Every term in equation D.4 has an uncertainty. δE_m is the correctional term and is used to correct the mechanical energy. It can be neglected because it is so small and/or because the conditions that need correction does not occur. The absolute systematic uncertainty in the mechanical energy is:

$$e_{E_{m_s}} = \pm\sqrt{e^2_{E_{m,ps}} + e^2_{E_{m,kin_s}} + e^2_{E_{m,pot_s}} + e^2_{E_{m,T_s}}} \tag{D.5}$$

The relative systematic uncertainty is given by:

$$f_{E_{m_s}} = \frac{e_{E_{m_s}}}{E_m} \tag{D.6}$$

Mechanical pressure energy

The mechanical pressure is given by:

$$E_{m,p} = \bar{a}(p_{1-1} - p_{2-1}) \tag{D.7}$$

Where $\bar{a}$ is the isothermal coefficient which can be found by formula or table values given in IEC 41. p_{1-1} is the pressure at the thermometer at the inlet. p_{2-1} is the pressure at the thermometer at the outlet.

$$p_{1-1} = p_{1-1,measured} + \frac{\bar{\rho} g \Delta z_{1-1}}{1000} \tag{D.8}$$

$$p_{2-1} = p_{atm} + \frac{\bar{\rho} g h_{2-1}}{1000} \tag{D.9}$$

Divide by 1000 to get the unit kPa because the pressure was measured in kPa.

$$E_{m,p} = f(\bar{a}, p_{1-1}, \bar{\rho}, \Delta z_{1-1}, h_{2-1}, p_{atm}) \tag{D.10}$$

The uncertainty in $E_{m,pressure}$ is given by equation D.11.

$$e_{Em,p_s} = \sqrt{e^2_{Em,p,\bar{a}} + e^2_{Em,p,p_{1-1}} + e^2_{Em,p,\bar{\rho}} + e^2_{Em,p,\Delta z_{1-1}} + e^2_{Em,p,h_{2-1}} + e^2_{Em,p,p_{atm}}} \tag{D.11}$$

$$e^2_{Em,p,\bar{a}} = ((p_{1-1} - p_{2-1})e_{\bar{a}})^2 \tag{D.12}$$

$$e^2_{Em,p,p_{1-1}} = (\bar{a}e_{p,1-1,meas})^2 \tag{D.13}$$

$$e^2_{Em,p,\bar{\rho}} = \left(\frac{g(\Delta z_{1-1} - h_{2-1})}{1000} e_{\bar{\rho}}\right)^2 \tag{D.14}$$

$$e^2_{Em,p,\Delta z_{1-1}} = \left(\frac{\bar{\rho} g}{1000} e_{\Delta z_{1-1}}\right)^2 \tag{D.15}$$

$$e^2_{Em,p,h_{2-1}} = \left(\frac{\bar{\rho} g}{1000} e_{h_{2-1}}\right)^2 \tag{D.16}$$

$$e^2_{Em,p,p_{atm}} = (\bar{a}e_{p,atm})^2 \tag{D.17}$$

with $e_{\bar{a}} = \sqrt{e^2_{\bar{a}_{table}} + e^2_{\bar{a}_{temp}}}$.

where

$e_{\bar{a}_{table}}$ is the uncertainty in $\bar{a}$ of the tabulated values.

$e_{\bar{a}_{temp}}$ is the uncertainty in $\bar{a}$ related to the uncertainty in the temperature. (Can be neglected if ΔT is small).

$e_{p,1-1,meas}$ and $e_{p,atm}$ are related to the uncertainty in the measurement equipment.

Mechanical kinetic energy

The mechanical kinetic energy is given by:

$$E_{m,kin} = \frac{1}{2}\left(c_{1-1}^2 - c_{2-1}^2\right) \tag{D.18}$$

$$E_{m,kin} = f(c_{1-1}, c_{2-1}) \tag{D.19}$$

The uncertainty in $E_{m,kinetic}$ is given by equation D.20.

$$e_{Em,kin_s} = \sqrt{(c_{1-1}e_{c_{1-1}})^2 + (c_{2-1}e_{c_{2-1}})^2} \tag{D.20}$$

Mechanical potential energy

The mechanical potential energy is given by:

$$E_{m,pot} = \bar{g}(z_{1-1} - z_{2-1}) \tag{D.21}$$

$$E_{m,pot} = f(z_{1-1}, z_{2-1}) \tag{D.22}$$

The uncertainty in $E_{m,potential}$ is given by equation D.23.

$$e_{Em,pot_s} = \sqrt{(ge_{z_{1-1}})^2 + (ge_{z_{2-1}})^2} \tag{D.23}$$

According to IEC 41 the uncertainty related to the gravitation is negligible.

Mechanical thermal energy

The mechanical thermal energy is given by:

$$E_{m,T} = \bar{c_p}(T_{1-1} - T_{2-1}) = \bar{c_p}(\Delta T) \tag{D.24}$$

$$E_{m,T} = f(\bar{c_p}, T_{1-1}, T_{2-1}) \tag{D.25}$$

The uncertainty in $E_{m,thermal}$ is given by equation D.26.

$$e_{Em,T_s} = \sqrt{(\bar{c_p} e_{\Delta T})^2 + (\Delta T e_{\bar{c_p}})^2 + e_{E_{10}}^2 + e_{E_{20}}^2} \tag{D.26}$$

with $e_{\bar{c_p}} = \sqrt{e_{\bar{c_p}_{table}}^2 + e_{\bar{c_p}_{temp}}^2}$.

where

$e_{\bar{c_p}_{table}}$ is the uncertainty in $\bar{c_p}$ of the tabulated values.

$e_{\bar{c_p}_{temp}}$ is the uncertainty in $\bar{c_p}$ related to the uncertainty in the temperature. (Can be neglected if ΔT is small).

$e_{E_{10}}$ and $e_{E_{20}}$ are the uncertainties related to faulty exploration of the energy distribution. Meaning there were no velocity measurements.

$e_{\Delta T}$ are related to the uncertainty in the measurement equipment.

D.2.2 Hydraulic energy

In this section the systematic hydraulic energy uncertainty will be derived. The hydraulic energy is given by the equation

$$E_h = E_{h,pressure} + E_{h,kinetic} + E_{h,potential} \tag{D.27}$$

Every term in equation D.27 has an uncertainty. The absolute systematic uncertainty in the hydraulic energy is:

$$e_{E_{h_s}} = \pm\sqrt{e_{E_{h,p_s}}^2 + f_{E_{h,kin_s}}^2 + f_{E_{h,pot_s}}^2} \tag{D.28}$$

The relative systematic uncertainty is given by:

$$f_{E_{h_s}} = \frac{e_{E_{h,s}}}{E_h} \tag{D.29}$$

Hydraulic pressure

The hydraulic potential energy is given by:

$$E_{h,p} = \frac{1}{\bar{\rho}}(p_1 - p_2) \tag{D.30}$$

$$E_{h,p} = f(\bar{\rho}, p_1, p_2) \tag{D.31}$$

Where p_1 is the pressure at the inlet of the turbine. p_2 is the pressure at the outlet.

$$p_1 = p_{1,meas} + \frac{\bar{\rho} g \Delta z_1}{1000} \tag{D.32}$$

$$p_2 = p_{atm} + \frac{\bar{\rho} g h2}{1000} \tag{D.33}$$

The uncertainty in $E_{h,p}$ is given by equation D.34.

$$e_{Eh,p_s} = \sqrt{e^2_{Eh,p,p_{1,meas}} + e^2_{Eh,p,\bar{\rho}} + e^2_{Eh,p,\Delta z_1} + e^2_{Eh,p,h_2} + e^2_{Eh,p,p_{atm}}} \tag{D.34}$$

$$e^2_{Eh,p,p_{1,meas}} = (\frac{1}{\bar{\rho}} e_{p,1-1,meas})^2 \tag{D.35}$$

$$e^2_{Eh,p,\bar{\rho}} = \left(\frac{p_{1,meas} - p_{atm}}{\bar{\rho}^2} e_{\bar{\rho}}\right)^2 \tag{D.36}$$

$$e^2_{Eh,p,\Delta z_1} = \left(\frac{\bar{\rho} g}{1000} e_{\Delta z_1}\right)^2 \tag{D.37}$$

$$e^2_{Eh,p,h_2} = \left(\frac{\bar{\rho} g}{1000} e_{h_2}\right)^2 \tag{D.38}$$

$$e^2_{Eh,p,p_{atm}} = \left(\frac{1}{\bar{\rho}} e_{p,atm}\right)^2 \tag{D.39}$$

where

$e_{\bar{\rho}}$ is related to the uncertainty in the density.

$e_{p,1}$ and $e_{p,atm}$ are related to the uncertainty in the measurement equipment.

Hydraulic kinetic energy

The hydraulic kinetic energy is given by:

$$E_{h,kin} = \frac{1}{2}(c_1^2 - c_2^2) \tag{D.40}$$

$$E_{h,kin} = f(c_1, c_2) \tag{D.41}$$

c_1 and c_2 are the velocity at the inlet and outlet of the turbine, respectively. When the velocity is not measured the velocities can be found by the volume flow rate.

$$Q = \frac{P_{turb} \cdot 10^6}{\bar{\rho} E_m} \tag{D.42}$$

where $\bar{\rho} = \frac{\rho_1 + \rho_2}{2}$ and $P_{turb} = \frac{P_{gen}}{\eta_{gen}}$. The velocity is then found by dividing the volume flow rate with the inlet or outlet area.

$$c = \frac{Q}{A} \tag{D.43}$$

Where $A_1 = \frac{\pi D_1^2}{4}$ and $A_2 = W_2 \cdot L_2$

$$E_{h,kin} = f(P_g, \bar{\rho}, E_m, D_1, W_2, L_2) \tag{D.44}$$

The uncertainty in $E_{h,kin}$ is given by equation D.45.

$$e_{Eh,kin} = \sqrt{(c_1 e_{c_1})^2 + (c_2 e_{c_2})^2} \tag{D.45}$$

The absolute uncertainty in the inlet velocity is:

$$e_{c1} = \sqrt{\left(\frac{e_{P_g}}{\eta_g \bar{\rho} E_m A_1}\right)^2 + \left(\frac{P_g \cdot 10^6}{\eta_g \bar{\rho}^2 E_m A_1} e_{\bar{\rho}}\right)^2 + \left(\frac{P_g \cdot 10^6}{\eta_g \bar{\rho} E_m^2 A_1} e_{E_m}\right)^2 + \left(\frac{P_g \cdot 10^6}{\eta_g \bar{\rho} E_m A_1^2} e_{A_1}\right)^2} \tag{D.46}$$

where

$$e_{A_1} = \frac{\pi D_1}{2} e_{D_1} \tag{D.47}$$

The absolute uncertainty in the outlet velocity is:

$$e_{c2} = \sqrt{\left(\frac{e_{P_g}}{\eta_g \bar{\rho} E_m A_2}\right)^2 + \left(\frac{P_g \cdot 10^6}{\eta_g \bar{\rho}^2 E_m A_2} e_{\bar{\rho}}\right)^2 + \left(\frac{P_g \cdot 10^6}{\eta_g \bar{\rho} E_m^2 A_2} e_{E_m}\right)^2 + \left(\frac{P_g \cdot 10^6}{\eta_g \bar{\rho} E_m A_2^2} e_{A_2}\right)^2} \tag{D.48}$$

where

$$e_{A_2} = A_2 \sqrt{\left(\frac{e_W}{W}\right)^2 + \left(\frac{e_L}{L}\right)^2} \tag{D.49}$$

Hydraulic potential energy

The hydraulic potential energy is given by:

$$E_{h,pot} = \bar{g}(z_1 - z_2) \tag{D.50}$$

$$E_{h,pot} = f(\bar{g}, z_1, z_2) \tag{D.51}$$

The uncertainty in $E_{h,pot}$ is given by equation D.52.

$$e_{Eh,pot_s} = \sqrt{(g e_{z_1})^2 + (g e_{z_2})^2} \tag{D.52}$$

According to IEC 41 [10] the uncertainty related to the gravitation is negligible.

D.2.3 Given and calculated uncertainties

Some of the uncertainties are given by IEC 41.

Variable	Term	Value
Isothermal coefficient, relative, table	$f_{\bar{a}_{table}}$	±0.2%
Isothermal coefficient, absolute, temp.	$e_{\bar{a}_{temp}}$	$\pm 0.00185 \cdot 10^{-3} m^3/kg$
Specific heat capacity, relative, table	$f_{\bar{cp}_{table}}$	±0.5%
Specific heat capacity, absolute, temp.	$e_{\bar{cp}_{temp}}$	$\pm 0.5 Jkg^{-1}K^{-1}$
Density, relative	$f_{\bar{\rho}_{table}}$, $f_{\bar{\rho}_{temp}}$	±0.1%
Temperature difference, absolute	$e_{\Delta T}$	$\pm 0.001 K$
Faulty exploration of energy distribution, inlet	$e_{E_{10}}$	±0.2% of Em
Faulty exploration of energy distribution, outlet	$e_{E_{20}}$	±0.6% of Em

Table D.1: Systematic uncertainties given by IEC41

Some are found by calibration.

Variable	Term	Value
Pressure sensor, Digiquartz 1	e_{p_1}	1.25
Pressure sensor, Digiquartz 2	$e_{p_{1-1}}$	1.90
Pressure sensor, 5 bar	$e_{p_{atm}}$	0.011363
Temperature sensor, Seabird SBE38	e_T	0.001

Table D.2: Uncertainties in calibration

Some are assumed.

Variable	Term	Value
Error in height values in technical sketches 1	e_z	0.1
Height from deck to water surface	$e_{h_{surface}}$	0.1
Height from thermometer to bottom channel	$e_{h_{sensor}}$	0.01
Inlet diameter	e_T	0.01
Inlet width	e_T	0.1

Table D.3: Assumed uncertainties

D.3 Random uncertainty

In this section the random uncertainty will be derived. The total random uncertainty consists of the random uncertainty in the mechanical and hydraulic energy. According

to IEC 41 some of the random uncertainties can be set to zero. These uncertainties can be found in table D.4. The random uncertainty for the temperature and pressure depends on the measured values. To find these uncertainties the standard deviation was calculated, as in equation 2.6.

Variable	f	Value
Heights	f_{z_r}	~ 0%
Density	f_{ρ_r}	~ 0%
Isothermal coefficient	$f_{\bar{a}_r}$	~ 0%
Heat capacity	$f_{c_{pr}}$	~ 0%
Gravity	f_{g_r}	~ 0%
Generator output	$f_{P_{gen_r}}$	±0.1%

Table D.4: Random uncertainty according to IEC 41

Mechanical pressure energy

$$e_{Em,p_r} = \sqrt{e^2_{p,1-1_r} + e^2_{p,atm_r}} \tag{D.53}$$

Mechanical kinetic energy

$$e_{Em,kin_r} = \sqrt{e^2_{c,1-1_r} + e^2_{c,2-1_r}} \tag{D.54}$$

Mechanical potential energy

$$e_{Em,pot_r} = \sqrt{e^2_{z,1-1_r} + e^2_{z,2-1_r}} = 0 \tag{D.55}$$

Mechanical thermal energy

$$e_{Em,T_r} = \sqrt{e^2_{T,1-1_r} + e^2_{T,2-1_r}} \tag{D.56}$$

Mechanical energy

$$f_{Em_r} = \frac{e_{Em_r}}{E_m} = \frac{\sqrt{e^2_{Em,p_r} + e^2_{Em,kin_r} + e^2_{Em,pot_r} + e^2_{Em,T_r}}}{E_m} \tag{D.57}$$

Hydraulic pressure energy

$$e_{Eh,p_r} = \sqrt{e^2_{p,1_r} + e^2_{p,atm_r}} \tag{D.58}$$

Hydraulic kinetic energy

$$e_{Em,kin_r} = \sqrt{e_{c,1_r}^2 + e_{c,2_r}^2} \tag{D.59}$$

Where $e_{c,1_r} = e_{c,2_r} = e_{Q_r} = e_{P_{gen_r}}$

Hydraulic potential energy

$$e_{Eh,pot_r} = \sqrt{e_{z,1_r}^2 + e_{z,2_r}^2} = 0 \tag{D.60}$$

Hydraulic energy

$$f_{Eh_r} = \frac{e_{Eh_r}}{E_h} = \frac{\sqrt{e_{Eh,p_r}^2 + e_{Eh,kin_r}^2 + e_{Eh,pot_r}^2}}{E_h} \tag{D.61}$$

Appendix E

Temperature plots

In the figures below, the temperature in every measurement point is plotted. The height is the height from the channel bottom to the temperature sensor. ID=01 is the sensor which measured the inlet temperature, ID=02, ID=04 and ID=05 measured the outlet temperature.

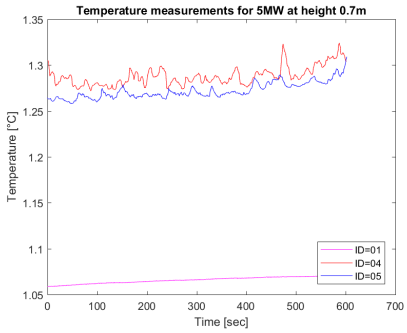

Figure E.1: Temperature measurements: 1 injector, 5MW, h=0,7m

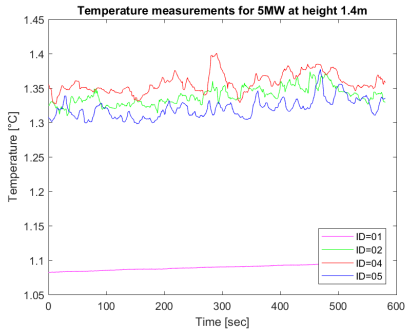

Figure E.2: Temperature measurements: 1 injector, 5MW, h=1,4m

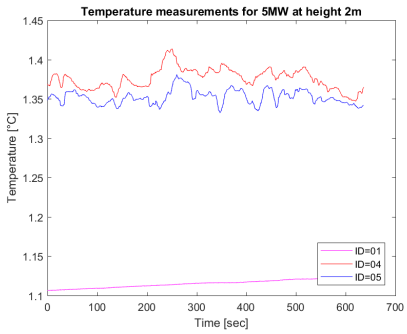

Figure E.3: Temperature measurements: 1 injector, 5MW, h=2m

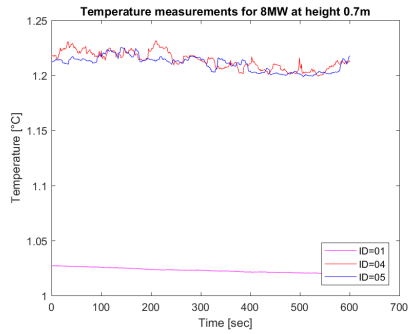

Figure E.4: Temperature measurements: 1 injector, 8MW, h=0,7m

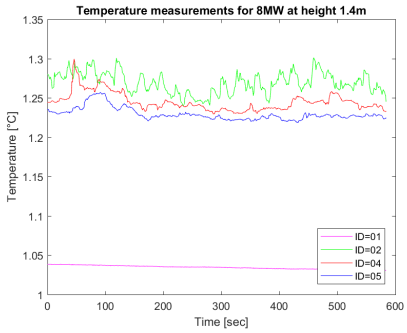

Figure E.5: Temperature measurements: 1 injector, 8MW, h=1,4m

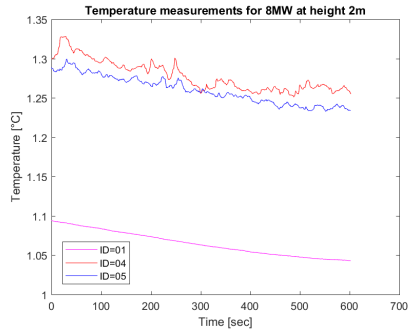

Figure E.6: Temperature measurements: 1 injector, 8MW, h=2m

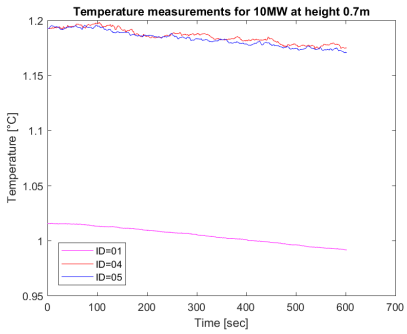

Figure E.7: Temperature measurements: 1 injector, 10W, h=0,7m

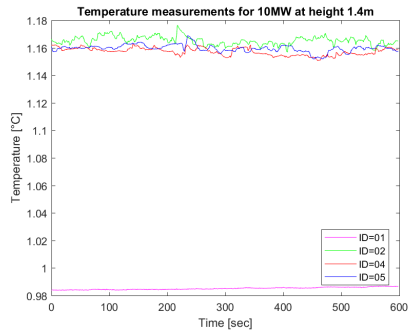

Figure E.8: Temperature measurements: 1 injector, 10MW, h=1,4m

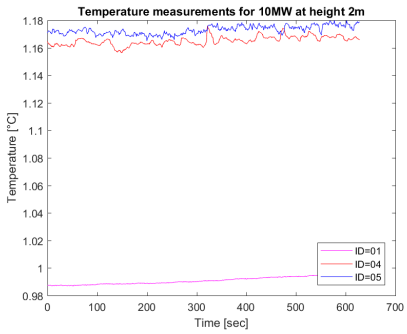

Figure E.9: Temperature measurements: 1 injector, 10MW, h=2m

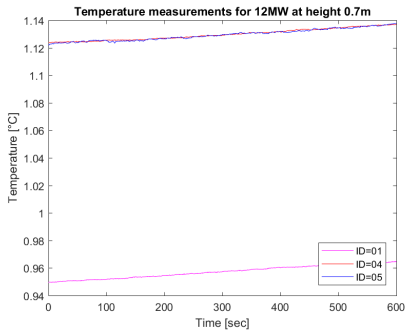

Figure E.10: Temperature measurements: 2 injector, 12MW, h=0,7m

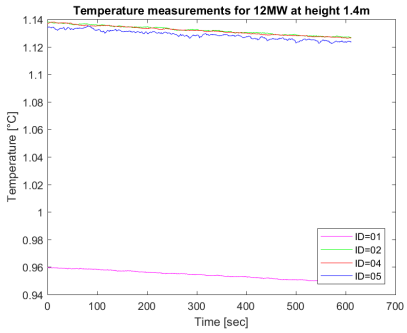

Figure E.11: Temperature measurements: 2 injector, 12MW, h=1,4m

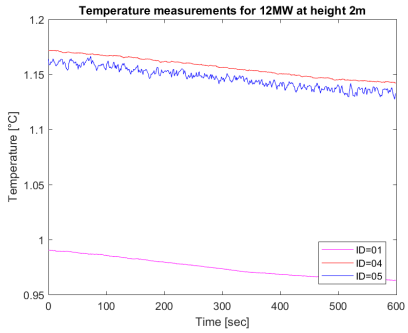

Figure E.12: Temperature measurements: 2 injector, 12MW, h=2m

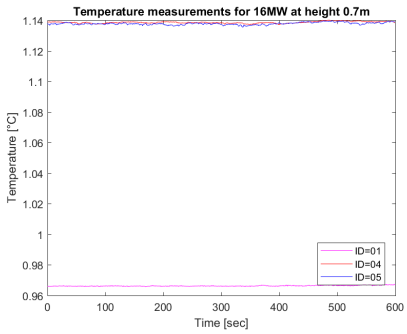

Figure E.13: Temperature measurements: 2 injector, 16MW, h=0,7m

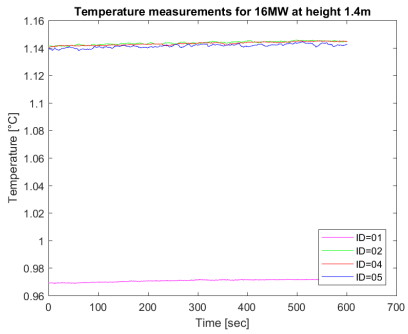

Figure E.14: Temperature measurements: 2 injector, 16MW, h=1,4m

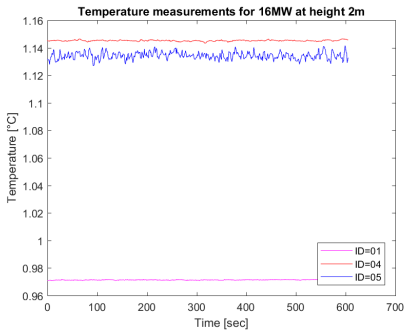

Figure E.15: Temperature measurements: 2 injector, 16MW, h=2m

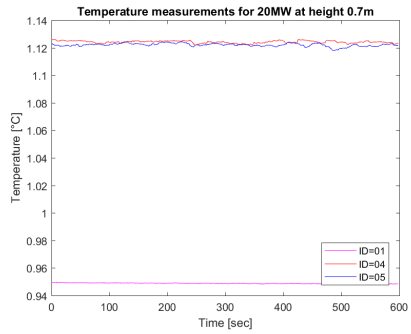

Figure E.16: Temperature measurements: 2 injector, 20MW, h=0,7m

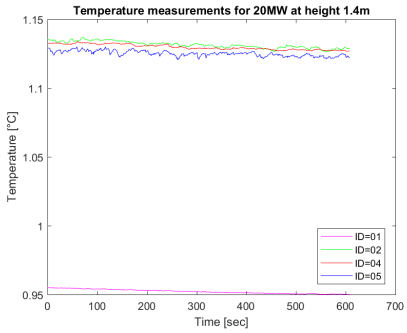

Figure E.17: Temperature measurements: 2 injector, 20MW, h=1,4m

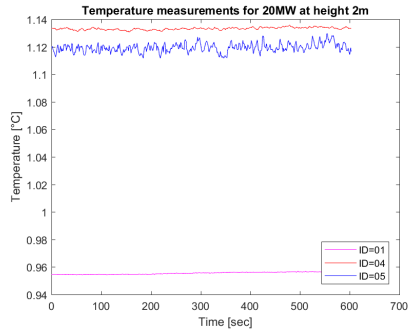

Figure E.18: Temperature measurements: 2 injector, 20MW, h=2m

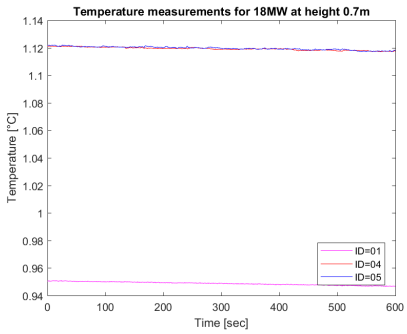

Figure E.19: Temperature measurements: 3 injector, 18MW, h=0,7m

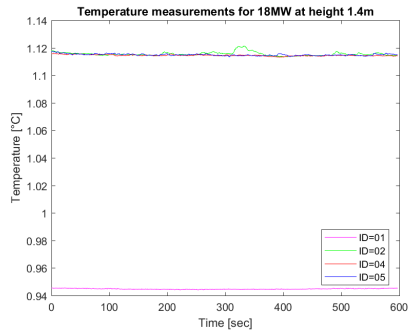

Figure E.20: Temperature measurements: 3 injector, 18MW, h=1,4m

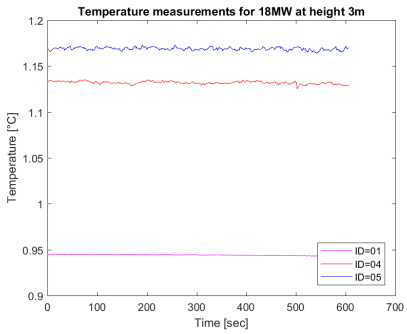

Figure E.21: Temperature measurements: 3 injector, 18MW, h=3m

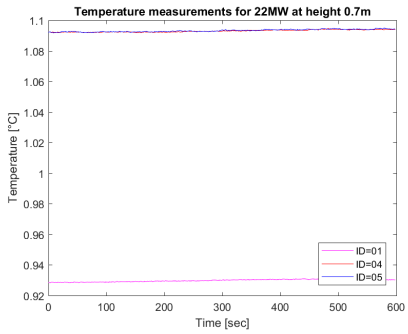

Figure E.22: Temperature measurements: 3 injector, 22MW, h=0,7m

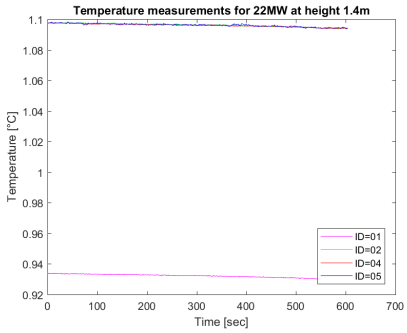

Figure E.23: Temperature measurements: 3 injector, 22MW, h=1,4m

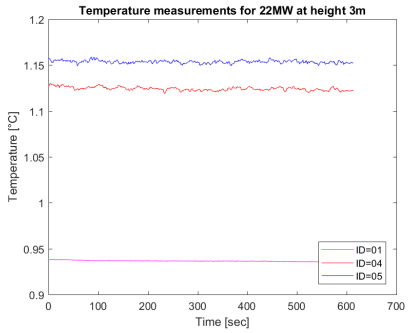

Figure E.24: Temperature measurements: 3 injector, 22MW, h=3m

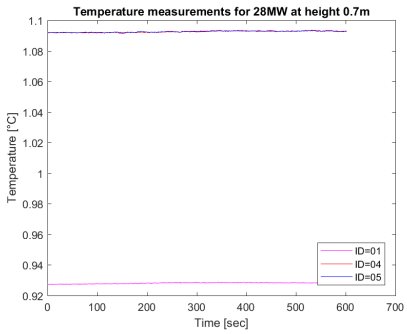

Figure E.25: Temperature measurements: 3 injector, 28MW, h=0,7m

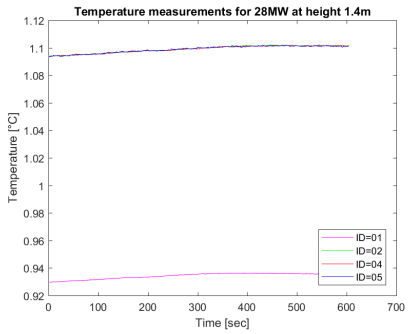

Figure E.26: Temperature measurements: 3 injector, 28MW, h=1,4m

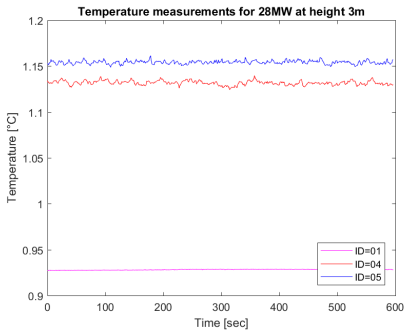

Figure E.27: Temperature measurements: 3 injector, 28MW, h=3m

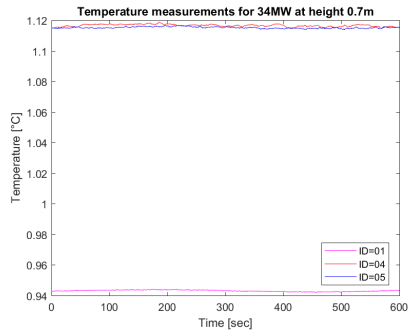

Figure E.28: Temperature measurements: 6 injector, 34MW, h=0,7m

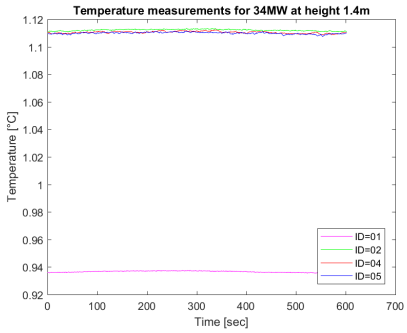

Figure E.29: Temperature measurements: 6 injector, 34MW, h=1,4m

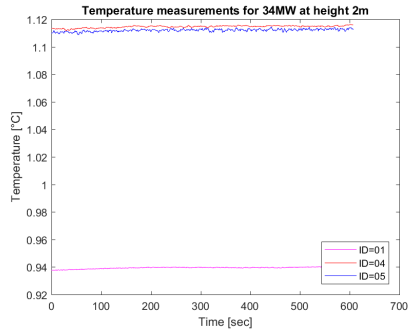

Figure E.30: Temperature measurements: 6 injector, 34MW, h=2m

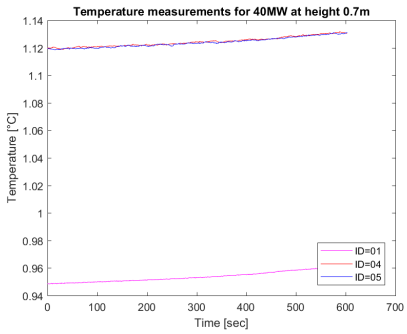

Figure E.31: Temperature measurements: 6 injector, 40MW, h=0,7m

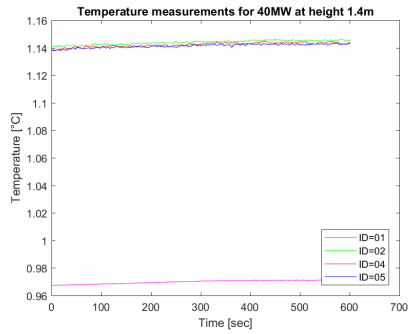

Figure E.32: Temperature measurements: 6 injector, 40MW, h=1,4m

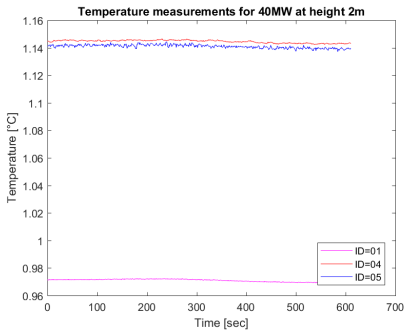

Figure E.33: Temperature measurements: 6 injector, 40MW, h=2m

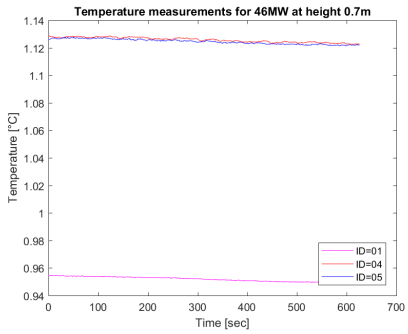

Figure E.34: Temperature measurements: 6 injector, 46MW, h=0,7m

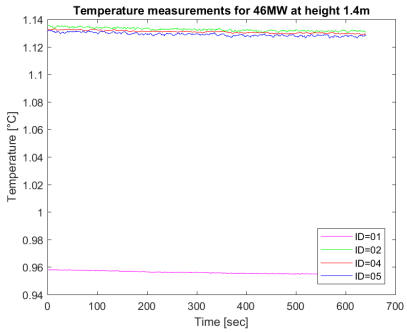

Figure E.35: Temperature measurements: 6 injector, 46MW, h=1,4m

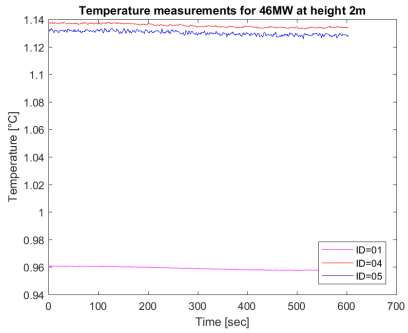

Figure E.36: Temperature measurements: 6 injector, 46MW, h=2m

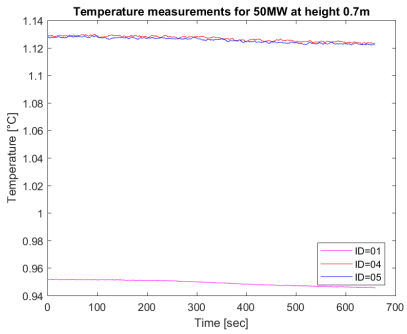

Figure E.37: Temperature measurements: 6 injector, 50MW, h=0,7m

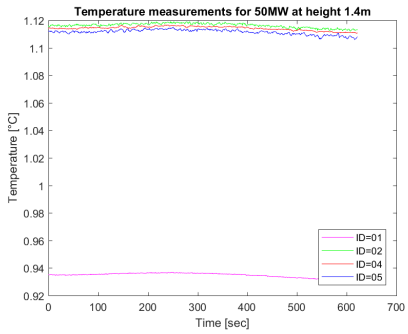

Figure E.38: Temperature measurements: 6 injector, 50MW, h=1,4m

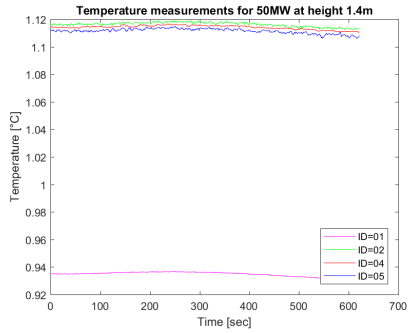

Figure E.39: Temperature measurements: 6 injector, 50MW, h=2m

Appendix F

Uncertainty in the calculated mechanical energy

This appendix contains tables with the uncertainty in the measured mechanical energy for all power settings and all 7 measurement points.

Measurement point	$e_{Em,pressure}$ $[J/kg]$	$e_{Em,kinetic}$ $[J/kg]$	$e_{Em,potential}$ $[J/kg]$	$e_{Em,thermal}$ $[J/kg]$	$e_{Em,total}$ $[J/kg]$
1	13,4751	0	1,3886	37,4054	39,7827
2	13,4741	0	1,3886	37,7730	40,1283
3	13,4905	0	1,3886	36,7915	39,2114
4	13,4917	0	1,3886	36,3640	38,8109
5	13,4894	0	1,3886	37,2020	39,5964
6	13,5031	0	1,3886	36,5292	38,9697
7	13,5016	0	1,3886	37,0652	39,4722

Table F.1: Uncertainty in mechanical energy for turbine power P_t =5MW

Measurement point	$e_{Em,pressure}$ $[J/kg]$	$e_{Em,kinetic}$ $[J/kg]$	$e_{Em,potential}$ $[J/kg]$	$e_{Em,thermal}$ $[J/kg]$	$e_{Em,total}$ $[J/kg]$
1	13,4691	0	1,3886	38,1215	40,4548
2	13,4689	0	1,3886	38,1952	40,5242
3	13,4856	0	1,3886	37,0950	39,4946
4	13,4841	0	1,3886	37,6593	40,0246
5	13,4832	0	1,3886	38,0216	40,3654
6	13,4961	0	1,3886	37,6042	39,9768
7	13,4950	0	1,3886	38,0237	40,3714

Table F.2: Uncertainty in mechanical energy for turbine power P_t =8MW

Measurement point	$e_{Em,pressure}$ $[J/kg]$	$e_{Em,kinetic}$ $[J/kg]$	$e_{Em,potential}$ $[J/kg]$	$e_{Em,thermal}$ $[J/kg]$	$e_{Em,total}$ $[J/kg]$
1	13,4660	0	1,3886	38,3451	40,6646
2	13,4658	0	1,3886	38,4025	40,7186
3	13,4798	0	1,3886	38,3655	40,6884
4	13,4794	0	1,3886	38,5572	40,8690
5	13,4794	0	1,3886	38,5002	40,8153
6	13,4912	0	1,3886	38,5089	40,8274
7	13,4917	0	1,3886	38,3232	40,6525

Table F.3: Uncertainty in mechanical energy for turbine power P_t =10MW

Measurement point	$e_{Em,pressure}$ $[J/kg]$	$e_{Em,kinetic}$ $[J/kg]$	$e_{Em,potential}$ $[J/kg]$	$e_{Em,thermal}$ $[J/kg]$	$e_{Em,total}$ $[J/kg]$
1	13,4508	0	1,3886	38,5080	40,8132
2	13,4508	0	1,3886	38,5144	40,8192
3	13,4649	0	1,3886	38,3831	40,70
4	13,4649	0	1,3886	38,3921	40,7085
5	13,4647	0	1,3886	38,4660	40,7782
6	13,4770	0	1,3886	38,2872	40,6137
7	13,4764	0	1,3886	38,520	40,8330

Table F.4: Uncertainty in mechanical energy for turbine power P_t =12MW

Measurement point	$e_{Em,pressure}$ $[J/kg]$	$e_{Em,kinetic}$ $[J/kg]$	$e_{Em,potential}$ $[J/kg]$	$e_{Em,thermal}$ $[J/kg]$	$e_{Em,total}$ $[J/kg]$
1	13,4461	0	1,3886	38,4990	40,8032
2	13,4460	0	1,3886	38,5184	40,8214
3	13,4599	0	1,3886	38,4870	40,7964
4	13,4599	0	1,3886	38,4991	40,8077
5	13,4598	0	1,3886	38,5398	40,8462
6	13,4718	0	1,3886	38,4625	40,7772
7	13,4711	0	1,3886	38,7237	51,0235

Table F.5: Uncertainty in mechanical energy for turbine power P_t =16MW

Measurement point	$e_{Em,pressure}$ $[J/kg]$	$e_{Em,kinetic}$ $[J/kg]$	$e_{Em,potential}$ $[J/kg]$	$e_{Em,thermal}$ $[J/kg]$	$e_{Em,total}$ $[J/kg]$
1	13,4330	0	1,3886	38,5036	40,8032
2	13,4330	0	1,3886	38,4942	40,7943
3	13,4468	0	1,3886	38,4994	40,8038
4	13,4467	0	1,3886	38,5230	40,8260
5	13,4467	0	1,3886	38,5132	40,8168
6	13,4794	0	1,3886	38,0923	40,4308
7	13,4816	0	1,3886	37,2277	39,6180

Table F.6: Uncertainty in mechanical energy for turbine power P_t =18MW

Measurement point	$e_{Em,pressure}$ $[J/kg]$	$e_{Em,kinetic}$ $[J/kg]$	$e_{Em,potential}$ $[J/kg]$	$e_{Em,thermal}$ $[J/kg]$	$e_{Em,total}$ $[J/kg]$
1	13,4512	0	1,3886	38,4436	40,7526
2	13,4511	0	1,3886	38,4941	40,8002
3	13,4652	0	1,3886	38,3518	40,6707
4	13,4652	0	1,3886	38,3924	40,7089
5	13,4649	0	1,3886	38,5045	40,8145
6	13,4770	0	1,3886	38,3910	40,7115
7	13,4762	0	1,3886	38,7237	41,0251

Table F.7: Uncertainty in mechanical energy for turbine power P_t =20MW

Measurement point	$e_{Em,pressure}$ $[J/kg]$	$e_{Em,kinetic}$ $[J/kg]$	$e_{Em,potential}$ $[J/kg]$	$e_{Em,thermal}$ $[J/kg]$	$e_{Em,total}$ $[J/kg]$
1	13,4188	0	1,3886	38,6359	40,9234
2	13,4188	0	1,3886	38,6304	40,9182
3	13,4326	0	1,3886	38,6160	40,9092
4	13,4326	0	1,3886	38,6194	40,9124
5	13,4326	0	1,3886	38,6158	40,9090
6	13,4656	0	1,3886	38,0509	40,3872
7	13,4674	0	1,3886	37,3618	39,7391

Table F.8: Uncertainty in mechanical energy for turbine power P_t =22MW

Measurement point	$e_{Em,pressure}$ $[J/kg]$	$e_{Em,kinetic}$ $[J/kg]$	$e_{Em,potential}$ $[J/kg]$	$e_{Em,thermal}$ $[J/kg]$	$e_{Em,total}$ $[J/kg]$
1	13,3846	0	1,3886	38,4982	40,7823
2	13,3847	0	1,3886	38,4969	40,7810
3	13,3985	0	1,3886	38,4913	40,7802
4	13,3985	0	1,3886	38,4939	40,7827
5	13,3985	0	1,3886	38,4929	40,7818
6	13,4324	0	1,3886	37,5679	39,9212
7	13,4338	0	1,3886	37,0470	39,4319

Table F.9: Uncertainty in mechanical energy for turbine power P_t =28MW

Measurement point	$e_{Em,pressure}$ $[J/kg]$	$e_{Em,kinetic}$ $[J/kg]$	$e_{Em,potential}$ $[J/kg]$	$e_{Em,thermal}$ $[J/kg]$	$e_{Em,total}$ $[J/kg]$
1	13,3586	0	1,3886	38,1966	40,4890
2	13,3585	0	1,3886	38,2288	40,5193
3	13,3725	0	1,3886	38,1471	40,4470
4	13,3724	0	1,3886	38,1851	40,4828
5	13,3723	0	1,3886	38,1997	40,4964
6	13,3843	0	1,3886	38,1574	40,4606
7	13,3842	0	1,3886	38,2186	40,5183

Table F.10: Uncertainty in mechanical energy for turbine power P_t =34MW

Measurement point	$e_{Em,pressure}$ $[J/kg]$	$e_{Em,kinetic}$ $[J/kg]$	$e_{Em,potential}$ $[J/kg]$	$e_{Em,thermal}$ $[J/kg]$	$e_{Em,total}$ $[J/kg]$
1	13,31058	0	1,3886	38,1166	40,3977
2	13,3105	0	1,3886	38,1298	40,4102
3	13,3246	0	1,3886	38,0347	40,4102
4	13,3245	0	1,3886	38,0748	40,3251
5	13,3244	0	1,3886	38,0968	40,3629
6	13,3364	0	1,3886	38,0455	40,3392
7	13,3362	0	1,3886	38,1305	40,4193

Table F.11: Uncertainty in mechanical energy for turbine power P_t =40MW

Measurement point	$e_{Em,pressure}$ $[J/kg]$	$e_{Em,kinetic}$ $[J/kg]$	$e_{Em,potential}$ $[J/kg]$	$e_{Em,thermal}$ $[J/kg]$	$e_{Em,total}$ $[J/kg]$
1	13,2659	0	1,3886	37,8962	40,1751
2	13,2659	0	1,3886	37,9265	40,1205
3	13,2799	0	1,3886	37,8334	40,1205
4	13,2798	0	1,3886	38,7297	40,9667
5	13,2797	0	1,3886	37,9186	40,2007
6	13,2917	0	1,3886	37,3839	40,1296
7	13,2914	0	1,3886	37,9652	40,2486

Table F.12: Uncertainty in mechanical energy for turbine power P_t =46MW

Measurement point	$e_{Em,pressure}$ $[J/kg]$	$e_{Em,kinetic}$ $[J/kg]$	$e_{Em,potential}$ $[J/kg]$	$e_{Em,thermal}$ $[J/kg]$	$e_{Em,total}$ $[J/kg]$
1	13,2306	0	1,3886	37,7031	39,9813
2	13,2305	0	1,3886	37,7378	40,0139
3	13,2446	0	1,3886	37,6211	39,9085
4	13,2445	0	1,3886	37,6775	39,9617
5	13,2443	0	1,3886	37,7467	40,0269
6	13,2564	0	1,3886	37,6596	39,9488
7	13,2561	0	1,3886	37,8143	40,0946

Table F.13: Uncertainty in mechanical energy for turbine power P_t =50MW